THE ASTROPHYSICAL JOURNAL SUPPLEMENT SERIES, 63:721–748, 1987 March

HIGH-ENERGY PROCESSES IN SOLAR FLARES

R. J. MURPHY,[1] C. D. DERMER,[2] AND R. RAMATY
Laboratory for High Energy Astrophysics, NASA/Goddard Space Flight Center
Received 1986 June 9; accepted 1986 September 3

ABSTRACT

We have investigated in detail the production of gamma rays and neutrons by the interaction of high-energy flare-accelerated particles with the solar atmosphere. We have considered the production of neutral and charged pions, and we have evaluated the broad-band gamma-ray spectrum resulting from the decay of neutral pions, the bremsstrahlung of positrons and electrons from the decay of charged pions, and the annihilation in flight of positrons. We have also evaluated the 0.511 MeV gamma-ray line resulting from the annihilation of the positrons which survive annihilation in flight. The nuclear reactions which produce the pions also produce high-energy neutrons, and we have evaluated the spectrum and flux at the Earth of these particles. All of these calculations were performed in an isotropic, thick-target model using the best available nuclear data and models. We have used stochastic and shock-acceleration models for the acceleration of the primary particles, and we have considered the fluxes of secondary protons and neutrons. We compared the results, together with earlier calculations involving lower energy particles, with the following extensive observations of the 1982 June 3 flare: 10–120 MeV gamma rays, 0.511 and 2.2 MeV line emission, nuclear line emission, high-energy neutrons, and interplanetary charged particles. We have constructed a self-consistent interaction model for this flare in which the time-dependent fluxes are produced by two distinct particle populations with different acceleration and interaction time histories as well as different but time-independent energy spectra. We associate these two populations with first- and second-phase particle acceleration in solar flares.

Subject headings: gamma rays: general — nuclear reactions — particle acceleration — Sun: flares

I. INTRODUCTION

Interactions in the solar atmosphere of flare-accelerated particles produce a variety of detectable radiations. Of these, high-energy neutrons and broad-band gamma-ray emission extending to energies greater than 100 MeV are signatures of the highest energy processes taking place on the Sun. Both these emissions can be due to interactions involving pions. In the energy range from about 10 to 100 MeV, the thick-target spectrum of gamma rays from pion decay is exceptionally hard. Such a hard spectrum was observed (Forrest *et al.* 1985) after the impulsive phase of the 1982 June 3 flare with the gamma-ray spectrometer (GRS) on the *Solar Maximum Mission* (*SMM*). High-energy neutrons were also observed from this flare with ground-based neutron monitors (Debrunner *et al.* 1983; Efimov, Kocharov, and Kudela 1983; Iucci *et al.* 1984) and the *SMM*/GRS detector (Chupp *et al.* 1983). A variety of other related emissions were also seen: protons resulting from the decay of neutrons in interplanetary space (Evenson, Meyer, and Pyle 1983), gamma-ray lines at 0.511 MeV (Share *et al.* 1983) from positron annihilation and at 2.223 MeV (Prince *et al.* 1983) from neutron capture, an excess above the continuum between 4.1 and 6.4 MeV (Chupp *et al.* 1983) due to nuclear de-excitation lines, and interplanetary, energetic charged particles with a very hard proton spectrum (McDonald and Van Hollebeke 1985; Van Hollebeke, McDonald, and Trainor 1985).

In the present paper we have carried out a detailed study of high-energy processes in solar flares. We have calculated the production of neutrons and pions, incorporating isobaric and scaling models and a recent compilation of pion production data (Dermer 1986*a*, *b*). We have evaluated the spectra of neutrons, gamma rays from neutral pion decay, and secondary positrons and electrons from charged pion decay. We have subsequently calculated the gamma-ray emission resulting from the bremsstrahlung of the secondary positrons and electrons and the annihilation in flight of the positrons. We have performed our calculations in a thick-target model (e.g., Ramaty 1986) using the accelerated particle spectra expected from both stochastic acceleration (e.g., Forman, Ramaty, and Zweibel 1986) and shock acceleration (Ellison and Ramaty 1985). In this model, both the interacting primary and the secondary charged particles remain trapped at the Sun, but the neutrons and gamma rays are allowed to escape unattenuated, except for the 2.223 MeV line which is attenuated by Compton scattering in the photosphere (Wang and Ramaty 1974). These assumptions require that the interaction region be located above the photosphere. We further assume that the accelerated particles in the interaction region are isotropic. It was shown previously (Murphy and Ramaty 1985) that this relatively simple model is capable of accounting for many of the neutron and gamma-ray observations of solar flares.

[1]Also Department of Physics and Astronomy, University of Maryland, College Park.
[2]National Academy of Sciences–National Research Council Resident Research Associate.

Several previous studies on neutron and pion production in solar flares are available (e.g., Lingenfelter *et al.* 1965; Ramaty, Kozlovsky, and Lingenfelter 1975; Kocharov 1983). Most recently, Murphy and Ramaty (1985) have performed detailed calculations in an attempt to provide a self-consistent model for all the available neutron and gamma-ray observations from flares. However, they used relatively simple approximations at energies above the pion production threshold and did not consider in detail the recently developed shock-acceleration models. Efimov and Kocharov (1985) also studied neutron production, but they considered only proton-proton interactions and did not relate their calculations to gamma-ray production. Gamma-ray spectra from neutral pion decay were evaluated by Crannell, Crannell, and Ramaty (1979), but this study did not take into account the radiation produced by the secondary positrons and electrons. An estimate of the contribution of these secondaries was made by Ramaty *et al.* (1983*a*), but no differential photon spectra were calculated in this study.

We have constructed a self-consistent interaction model for the 1982 June 3 flare capable of accounting for all of the observed emissions mentioned above. Our analysis of the various observed time-dependent fluxes strongly suggests that the gamma rays and neutrons in this flare were produced by at least two distinct particle populations with different acceleration and interaction time histories. It was first suggested by Wild, Smerd, and Weiss (1963) that particle acceleration in flares may occur in at least two phases. Radio, X-ray (e.g., Vlahos *et al.* 1986) and recent gamma-ray (Forrest *et al.* 1981; Chupp 1984) observations showed that nonrelativistic electrons, as well as protons and relativistic electrons, are accelerated impulsively in the first phase by an as yet unknown mechanism. Second-phase acceleration, on the other hand, is extended in time and probably associated with a shock moving through the corona. We associate the two particle populations of the June 3 flare with these two acceleration phases. We find that the protons accelerated in the first phase have a much steeper spectrum and are more numerous than those accelerated in the second. We associate the flatter second-phase proton spectrum with the very hard proton spectrum observed in interplanetary space from the June 3 flare.

Gamma-ray emission that can be convincingly identified as pion decay radiation has so far been observed only from the 1982 June 3 flare. Emission above 10 MeV has been observed from many other flares, but it appears that in all of these cases this emission is predominantly bremsstrahlung of primary electrons. This follows from the fact that at these high energies flares are seen (Rieger *et al.* 1983) preferentially from sites close to the solar limb, requiring a highly beamed radiation pattern that is more likely due to ultrarelativistic electron bremsstrahlung (Petrosian 1985; Dermer and Ramaty 1986) than to pion decay. The spectrum of the radiation should also give information on its origin, but only in two cases (the flares of 1980 June 21 and 1982 June 3) were detailed >10 MeV spectra published (Forrest *et al.* 1985). For the 1980 June 21 flare the spectrum is much steeper than that expected from pion decay and hence is probably due to primary electron bremsstrahlung. This interpretation is consistent with the steep proton spectrum deduced (Ramaty *et al.* 1983*b*) from neutron observations (Chupp *et al.* 1982) which could not produce sufficient pions to account for the observed gamma rays. A steep photon spectrum, probably due to primary electron bremsstrahlung, was also observed during the impulsive phase of the June 3 flare, although at energies greater than about 70 MeV a pronounced flattening was seen. We find that the first-phase proton spectrum of this flare, even though much softer than that of the second phase, is hard enough to produce this flattening via pion decay.

In § II we discuss the acceleration mechanisms and the interaction model, in § III we present the relevant nuclear physics, in § IV we treat the bremsstrahlung and annihilation in flight including the effects of synchrotron losses, and in § V we present general numerical results. In § VI we apply these results to the June 3 flare and compare the conclusions with previous results obtained (Murphy and Ramaty 1985) for the June 21 flare. We summarize our conclusions in § VII.

II. ACCELERATION AND INTERACTION MODELS

In this section we discuss the energy spectra of the accelerated particles, the interaction model and the acceleration and interaction sites, and the composition of both the accelerated particles and the ambient medium.

a) Acceleration Models

The acceleration mechanisms that have been investigated in greatest detail for solar flares are stochastic acceleration and shock acceleration (e.g., Forman, Ramaty, and Zweibel 1986). For steady state stochastic acceleration in a region where the diffusion mean free path and escape time are independent of particle energy and species, the spectrum of nonrelativistic particles is given by (Ramaty 1979)

$$N_i(E) \propto C_i K_2\left[2(3p/m_p c\alpha T)^{1/2}\right], \qquad (1)$$

where $N_i(E)$ is the number of particles of species i per unit kinetic energy per nucleon E with abundance C_i, p is momentum per nucleon, m_p is the mass of the proton, α is the acceleration efficiency proportional to the ratio of the square of the velocity of the scattering centers to the diffusion mean free path, T is the escape time from the acceleration region, and K_2 is a modified Bessel function. The combination of parameters αT characterizes the steepness of the spectrum such that a larger value of αT corresponds to a harder spectrum. As just mentioned, equation (1) is a valid solution of the stochastic acceleration transport equation for nonrelativistic particles, and so its use for protons and nuclei up to about 100 MeV nucleon^{-1} is consistent with the underlying assumptions of this acceleration mechanism. For computational convenience we extend the range of use of equation (1) to the transrelativistic region. Here, however, this equation should be considered no more than a convenient mathematical expression. We do not use equation (1) for electrons, since these particles are ultrarelativistic at all the energies of interest.

The spectrum of particles resulting from diffusive shock acceleration is (e.g., Ellison and Ramaty 1985)

$$N_i \propto C_i(1/v)\, p^{-s} \exp\left(-E/E_{0i}\right). \qquad (2)$$

Here v is particle velocity, $s = (r+2)/(r-1)$, where r is the shock compression ratio, and the exponential term takes into account the effects of particle escape. Equation (2) is valid at all particle energies. The turnover kinetic energy, E_{0i}, for the various particle species depends on the distance to the escape boundary and the diffusion coefficient. If the diffusion coefficient is proportional to particle gyroradius,

$$v(E_{0i})\, R(E_{0i}) = v(E_{0p})\, R(E_{0p}). \qquad (3)$$

Here R is particle rigidity, E_{0p} is the proton turnover energy, and the E_{0i} are energy per nucleon for nuclei or energy for electrons.

The solid and dashed curves p in Figure 1 are fits to the observed (McDonald and Van Hollebeke 1985) proton spectrum from the 1980 June 21 flare with spectra obtained from equations (1) and (2), respectively. For the stochastic-acceleration spectrum, $\alpha T = 0.025$, while for the shock-acceleration spectrum, $s = 3.3$ and $E_{0p} = 30$ MeV. As can be seen, both spectra provide good fits to the data. The dashed curve e represents an electron spectrum obtained from equation (2) with the same s as that used to fit the proton data, an E_{0e} derived from equation (3), and injection conditions chosen to fit the observed relative proton and electron intensities (Ellison and Ramaty 1985). Since equation (1) is valid only for nonrelativistic particles, it cannot be used to fit the electron spectrum shown in Figure 1. In the ultrarelativistic regime, stochastic acceleration predicts a power law, but if αT is rigidity-independent, then the values of αT that fit the proton spectra produce ultrarelativistic electron spectra which are steeper than those observed (e.g., Ramaty 1979). Clearly, a complete stochastic-acceleration model should take into account the rigidity dependence of αT, but no attempts have yet been made (see Forman, Ramaty, and Zweibel 1986) to compare the theory with data in detail.

Whereas both stochastic and shock acceleration can fit the proton spectrum of the 1980 June 21 flare, shock acceleration provides a better fit to the proton spectrum of the 1982 June 3 flare. This can be seen in Figure 2, where the dashed curve p is a shock-acceleration spectrum with $s = 2.4$ and $E_{0p} \to \infty$ and the solid curve p is a stochastic-acceleration spectrum with $\alpha T = 0.04$. This value of αT is derived by fitting the spectrum of prompt gamma rays from the June 3 flare (see § VI). For the electron spectrum, curve e, $s = 2.4$ and $E_{0e} \to \infty$. This spectrum is normalized in such a way that the electron and proton fluxes are equal at 3 MeV. The absence of a turnover in the proton data sets a lower limit, $E_{0p} \gtrsim 300$ MeV. Equation (3) then implies that $E_{0e} \gtrsim 530$ MeV. We note that the interplanetary electron data for the June 3 flare are insufficient to define an electron spectrum over a broad range. The shape of curve e of Figure 2 is thus based only on theoretical considerations, and the interplanetary data are used only to set the normalization.

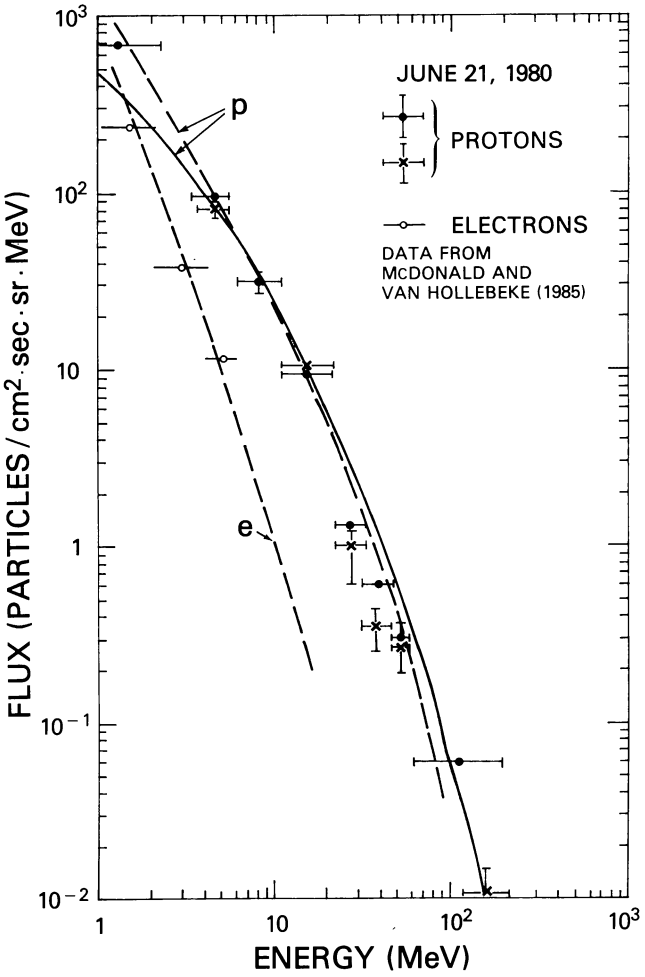

FIG. 1.—Interplanetary proton and electron observations (McDonald and Van Hollebeke 1985) of the 1980 June 21 flare. *Solid curve*: stochastic-acceleration spectrum with $\alpha T = 0.025$; *dashed curves*: shock-acceleration spectra with $s = 3.3$ and $E_{0p} = 30$ MeV for the protons and $E_{0e} = 59$ MeV for the electrons.

McDonald and Van Hollebeke (1985) have estimated the total number of interplanetary particles of energies greater than 30 MeV that escaped from these two flares. They find that $N_{p,\mathrm{esc}}(>30\ \mathrm{MeV})$ is approximately 1.5×10^{31} for the 1980 June 21 flare and 3×10^{32} for the 1982 June 3 flare.

b) Interaction Model

Neutron and gamma-ray production in solar flares most likely takes place in thick-target interactions (e.g., Murphy and Ramaty 1985); i.e., the nuclear reactions occur as the accelerated particles slow down and stop in the solar atmosphere. The interaction region is probably in the chromosphere, on the basis of several indirect arguments (Murphy and Ramaty 1985). The acceleration region is probably at higher altitudes, since, for efficient acceleration, a low ambient density is required. But there also could be multiple acceleration sites. An important distinguishing characteristic of the acceleration region is whether it is located in closed loops or

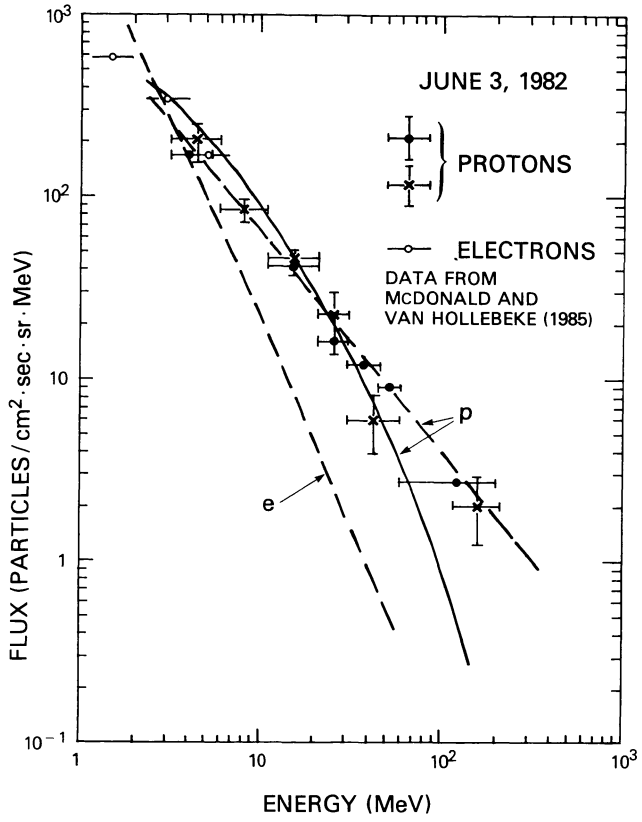

FIG. 2.—Interplanetary proton and electron observations (McDonald and Van Hollebeke 1985) of the 1982 June 3 flare. *Solid curve*: stochastic-acceleration spectrum with $\alpha T = 0.04$; *dashed curves*: shock-acceleration spectra with $s = 2.4$ and E_{0p} and E_{0e} tending to infinity.

open magnetic structures. The former would lead to strong gamma-ray emission without much particle escape into interplanetary space, while the latter could produce a large interplanetary particle event without a strong gamma-ray signal.

In our calculations we assume that accelerated particles with spectra given by either equation (1) or equation (2) impinge on the interaction region. The acceleration, as well as the transport of the particles from the acceleration site to the interaction region, could lead to significant anisotropies. As mentioned in § I, the limb brightening of the >10 MeV emission from flares is probably due to anisotropic distributions of relativistic electrons in flares. Dermer and Ramaty (1986) have shown that both downward-beamed electron distributions and distributions peaking at directions parallel to the photosphere are consistent with the >10 MeV bremsstrahlung data. The angular distribution of the protons could be best studied by comparing the 2.223 MeV line fluence with the flux of neutrons escaping from the Sun. Murphy and Ramaty (1985) have shown that for the 1982 June 3 flare the ratio of these emissions is consistent with an isotropic proton distribution. However, since this flare was close to the solar limb, a distribution peaking along the photosphere would also probably be consistent with the data (Hua and Lingenfelter 1987). Our calculations do take into account in detail the angular distribution of the neutrons as they are produced in the nuclear reactions. However, we found that it was beyond the scope of the present paper to consider the effects of the angular distribution of the primary protons, and therefore we have averaged all of our results over isotropic proton distributions. The particles are probably trapped in the interaction region by magnetic fields and isotropized by wave-particle interactions.

In the interaction region, the primary accelerated protons and heavier nuclei suffer Coulomb energy losses and elastic and inelastic nuclear collisions. Since the chromosphere is mostly neutral, we use the Coulomb loss rate in a neutral medium (Barkas and Berger 1964). We treat the effects of the nuclear collisions on the primary particles as a sudden loss using interaction cross sections for protons from Meyer (1972) and energy-independent destruction mean free paths of 13 and 5.2 g cm^{-2} for alpha particles and heavier nuclei, respectively. The nuclear collisions produce secondary protons, neutrons, and heavier nuclei. By comparing the secondary protons with the primary protons (see § V), we find that for most cases of interest the contribution of these protons to gamma-ray and neutron production is small. The contribution of secondary neutrons is even smaller, since the upward-moving neutrons produce essentially no nuclear reactions, while the downward-moving neutrons produce gamma rays which are expected to be significantly attenuated. We also ignore the secondary heavy nuclei because of their low relative abundance.

c) *Abundances*

The nuclear reaction yields also depend on the elemental compositions of both the ambient medium and the energetic particles. New information on the relative abundances of C, O, Ne, Mg, Si, and Fe in the chromosphere has been obtained from gamma-ray spectroscopy (Murphy *et al.* 1985*a*). The present calculations, however, are most sensitive to the abundances of He and heavier nuclei relative to H, which are not determined by the gamma-ray studies, and quite insensitive to the abundance differences between the chromosphere and photosphere suggested by the gamma-ray results. We assume, therefore, an ambient medium composition (Table 1) similar to that accepted for the photosphere (e.g., Cameron 1982).

Also shown in Table 1 are the 1980 June 21 and 1982 June 3 energetic particle compositions observed between 10 and 47 MeV nucleon^{-1} (Van Hollebeke, McDonald, and Trainor

TABLE 1

ELEMENTAL ABUNDANCES

Element	Ambient Medium	Energetic Particles	
		1980 June 21	1982 June 3
H	1.00	1.00	1.00
He	0.07	0.035	7.6×10^{-3}
C	4.2×10^{-4}	2.3×10^{-4}	7.2×10^{-5}
N	9.0×10^{-5}	7.0×10^{-5}	...
O	6.9×10^{-4}	4.4×10^{-4}	7.4×10^{-5}
Ne	1.0×10^{-4}	2.0×10^{-4}	6.4×10^{-5}
Mg	4.0×10^{-5}	7.9×10^{-5}	4.6×10^{-5}
Si	3.8×10^{-5}	6.6×10^{-5}	1.5×10^{-5}
Fe	3.4×10^{-5}	2.9×10^{-5}	1.9×10^{-4}

TABLE 2

REACTIONS OF PROTONS AND ALPHA PARTICLES INVOLVING PIONS

Reaction Number	Reaction	Reaction Number	Reaction
1	$p + p \rightarrow \pi^0 + X$	6.....	$p + \alpha \rightarrow \pi^0 + X$
2	$p + p \rightarrow \pi^+ + X$	7.....	$p + \alpha \rightarrow \pi^+ + X$
3	$p + p \rightarrow \pi^- + X$	8.....	$p + \alpha \rightarrow \pi^- + X$
4	$p + p \rightarrow n + X$	9.....	$p + \alpha \rightarrow n + X$
5	$p + p \rightarrow p + X$ (inelastic)	10.....	$p + \alpha \rightarrow p + X$ (inelastic)

1985). In the June 3 flare, He, C, and O are strongly depleted relative to H, and Fe is enhanced. On the other hand, these effects are essentially absent for the June 21 flare. It is well known (e.g., McGuire, von Rosenvinge, and McDonald 1986) that energetic particle abundances vary from flare to flare, and these data are typical examples. We perform our calculations for two accelerated particle compositions: a composition identical with that of the ambient medium, and another one identical with that observed from the June 3 flare. The results of these calculations should bracket those corresponding to the June 21 composition.

III. CROSS SECTIONS AND KINEMATICS

In this section we consider the reactions that produce secondary protons and neutrons, gamma rays from neutral pion decay, and positrons and electrons from charged pion decay. We discuss the reactions that involve pion production first.

a) Gamma-Ray, Positron, Electron, Proton and Neutron Production in Reactions Involving Pions

The relevant reactions are listed in Table 2. In this table, X denotes all other particles in the final state except the designated particle. The cross sections for reactions 1–4 are shown in Figure 3. All of these cross sections are inclusive in the sense that they include the multiplicity of the designated particle. The cross sections for pion production in p-p interactions, reactions 1–3, are fits (Dermer 1986*a*) to laboratory data. Below 1 GeV, the cross section for neutron production, reaction 4, was obtained by subtracting the cross section of the reaction $p + p \rightarrow \pi^+ + {}^2\mathrm{H}$ (Lock and Measday 1970) from the inclusive π^+ cross section. Between 1 and 2 GeV, the neutron inclusive cross section was determined from the measurements of Bugg *et al.* (1966). At higher energies we assume (as in Ramaty, Kozlovsky, and Lingenfelter 1975) that the inclusive neutron production cross section is 0.75 of the total inelastic p-p cross section, which is also shown in Figure 3 (Particle Data Group 1984). The inclusive cross section for proton production in inelastic p-p collisions, reaction 5, is the difference between twice the total inelastic p-p cross section and the sum of the inclusive neutron cross section and the deuterium production channel $p + p \rightarrow \pi^+ + {}^2\mathrm{H}$. This follows from baryon number conservation and is valid if additional antiproton and antineutron production (e.g., Tan and Ng 1982) is negligible, as is the case in the energy range of interest here.

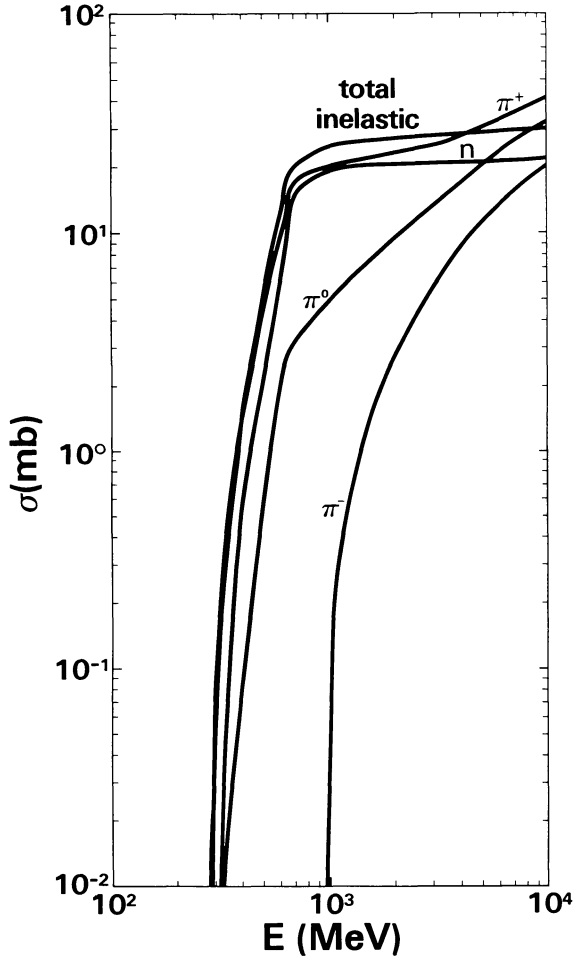

FIG. 3.—Inclusive cross sections for the production of neutrons, π^0, π^+, and π^- mesons in proton-proton interactions as a function of incident proton kinetic energy E. Also shown is the total inelastic p-p cross section.

The inclusive cross sections for reactions 6–8 of Table 2 are shown in Figure 4. At energies $\gtrsim 500$ MeV, where threshold effects are small, we assume that $\sigma_{p+\alpha\rightarrow\pi+X} = \frac{1}{2}S(\sigma_{p+p\rightarrow\pi+X} + \sigma_{p+n\rightarrow\pi+X})$ for the production of charged and neutral pions (see Cavallo and Gould 1971), where $S \approx 4^{3/4}$ is the shadowing factor in p-α collisions (Lebedev, Slavatinskii, and Tolkachev 1963; Orth and Buffington 1976). Assuming that $\sigma_{p+p\rightarrow\pi+X} \approx \sigma_{p+n\rightarrow\pi+X}$ on the basis of the near-equality of

the p-p and p-n inelastic cross section at energies $\gtrsim 2$ GeV (Particle Data Group 1984), we have $\sigma_{p+\alpha\to\pi+X} \approx 2.8\sigma_{p+p\to\pi+X}$ at high energies. At energies <1 GeV, the cross sections for π^+ and π^0 production in p-n collisions were estimated from cross-section data (Handler 1965; Lock and Measday 1970) for the reaction $p + n \to \pi^- + X$, applying branching ratios appropriate to the formation of an intermediate $\Delta_{3/2}$ resonance (see below). The cross sections were then interpolated between 1 and 2 GeV. This procedure gives an adequate fit to the data points shown in Figure 4. We assume that these branching ratios also hold at energies $\lesssim 500$ MeV where threshold effects are important, and take

$$\sigma_{p+\alpha\to\pi+X} = \sigma_{p+\alpha\to\pi^0+X}\left(\frac{\sigma_{p+p\to\pi+X} + \sigma_{p+n\to\pi+X}}{\sigma_{p+p\to\pi^0+X} + \sigma_{p+n\to\pi^0+X}}\right) \quad (4)$$

for the charged pion cross sections in p-α collisions at these energies. The values of $\sigma_{p+\alpha\to\pi^0+X}$ used in the above equation were estimated (Dermer 1986b) from measurements (Prokoshkin and Tiapkin 1958) at energies below 660 MeV. The cross sections for reactions 9 and 10 are from Meyer (1972).

We determine the laboratory system (LS) energy spectra of pions, neutrons, and protons produced in reactions 1–5 by combining isobar (Lindebaum and Sternheimer 1957; Stecker 1970) and scaling models (Badhwar, Stephens, and Golden 1977; Stephens and Badhwar 1981; Tan and Ng 1983) of high-energy interactions. An exception is the two-body channel $p + p \to \pi^+ + {}^2\mathrm{H}$ of reaction 2, for which we use center-of-momentum system (CMS) angular distribution data (see Meyer 1972). In the isobar model, intermediate isobaric states are formed which decay into nucleons and pions. From threshold to a few GeV, the data can be described reasonably well by assuming that secondary production proceeds through the formation of the $\Delta_{3/2}(1236)$ isobar, as was demonstrated in detail for π^0 production in p-p collisions by Dermer (1986b). We have now compared this model with charged pion, neutron, and proton production data at a variety of energies between threshold and 2 GeV. For example, in Figure 5a we show experimental data (Bugg *et al.* 1964) of CMS π^+ energy spectra at an incident proton energy of 970

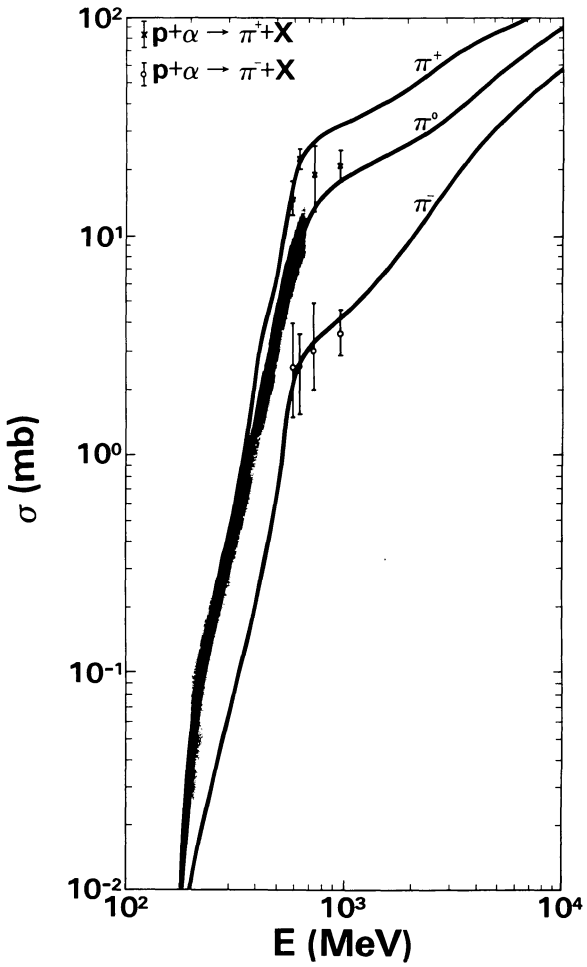

FIG. 4.

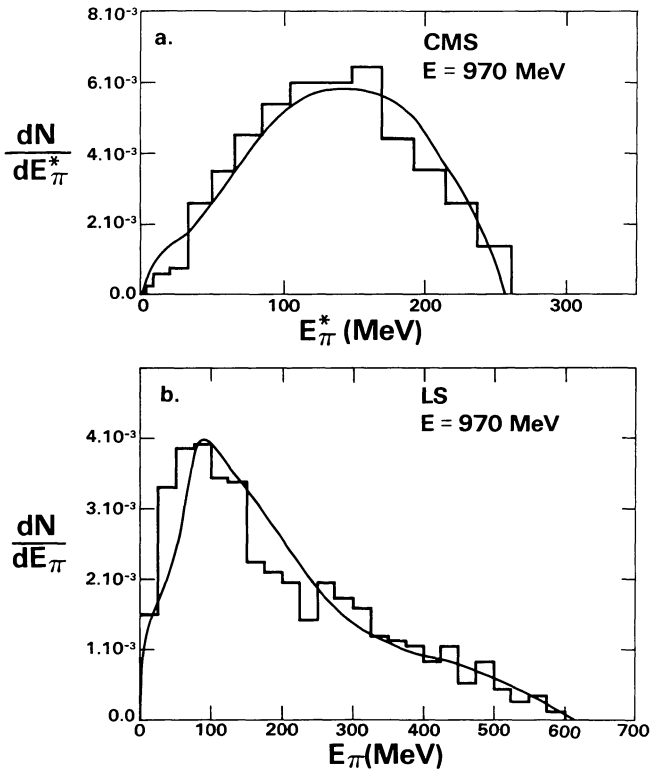

FIG. 5.

FIG. 4.—Inclusive cross sections for the production of π^0, π^+, and π^- mesons in proton–alpha particle interactions as a function of incident proton kinetic energy E. Shaded region represents the interpolated values of the $p + \alpha \to \pi^0 + X$ inclusive cross section at energies below 660 MeV, from Prokoshkin and Tiapkin (1958). Data points at 585, 630, 730, and 970 MeV are from Crawford *et al.* (1980), Kozodaev *et al.* (1960), Cochran *et al.* (1972), and Riddiford and Williams (1960), respectively.

FIG. 5.—Energy spectra of π^+ mesons produced in proton-proton interactions at 970 MeV. The histograms are the experimental data of Bugg *et al.* (1964), and the solid curves are from the isobar model (see text). (a) Energy spectra of π^+ mesons in the CMS. (b) Energy spectra of π^+ mesons in the LS. The solid curve is based on the assumption that the isobars travel along the directions of the incident protons in the CMS.

MeV. The model provides a good fit to the π^+ data. Calculations of secondary energy spectra in the LS depend on the angular distribution of the outgoing isobars in the CMS of the p-p system. But because the light pions are emitted with large Lorentz factors in the rest system of the isobar, their LS energy spectrum is relatively insensitive to this distribution. The assumption that the isobars are directed along the original directions of motion of the colliding protons (Stecker 1970) gives a good fit to the LS π^+ data (Bugg *et al.* 1964) in Figure 5*b*.

At energies $\gtrsim 10$ GeV, scaling representations provide a good description of pion data, but no good theory of secondary production exists between ~ 2 and 10 GeV. We have calculated secondary gamma-ray, positron, and electron spectra resulting from pion production in collisions of monoenergetic, isotropic protons with protons at rest, using the isobar model at energies near threshold and scaling representations for charged (Badhwar, Stephens, and Golden 1977) and neutral (Stephens and Badhwar 1981) pion production at high energies. The two models were joined smoothly between 3 and 7 GeV (Dermer 1986*b*), and the evaluation of the π-μ-e decay scheme followed previous work (Dermer 1986*a*). The results are shown in Figures 6–8 for the production of gamma rays, positrons, and electrons, respectively, at a variety of proton kinetic energies. The secondary spectra in p-α collisions were obtained from the p-p secondary spectra by multiplying the previous results by the ratio $\sigma_{p+\alpha\to\pi+X}/\sigma_{p+p\to\pi+X}$ at a given proton energy. The contributions from p-α collisions below the $p+p\to\pi+X$ threshold, α-α collisions, and collisions involving heavier nuclei introduced errors $\lesssim 10\%$ for the softest accelerated particle spectra used and were therefore neglected.

The LS angular distribution of the heavier neutrons is very sensitive to the assumed CMS angular distribution of the outgoing isobars. The forward-backward isobar angular distribution used for the pion calculations did not give a good fit to the LS neutron data (Bugg *et al.* 1964), as shown by curve 1 of Figure 9 at 970 MeV proton energy. We were able to

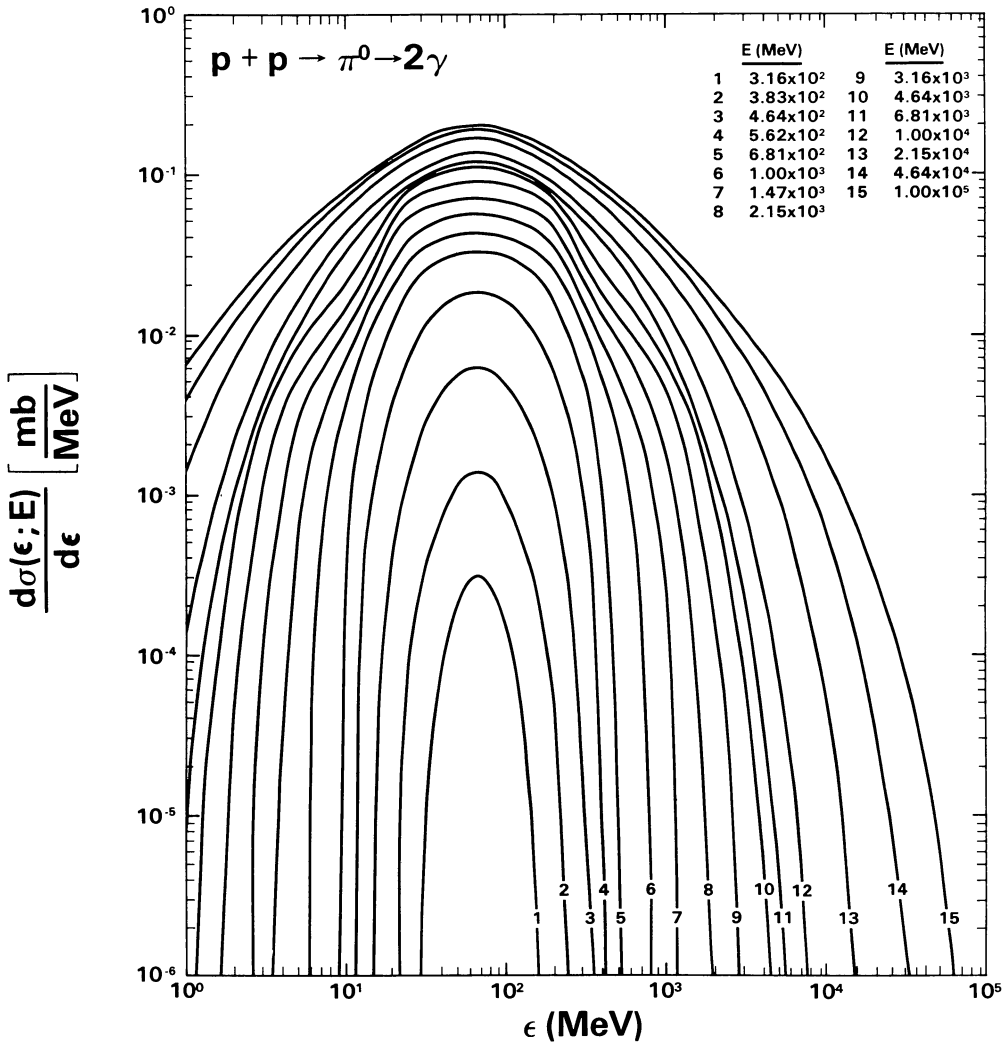

FIG. 6.—Energy spectra of gamma rays resulting from the decay of π^0 mesons produced in collisions of isotropic, monoenergetic protons with protons at rest, at a variety of proton kinetic energies.

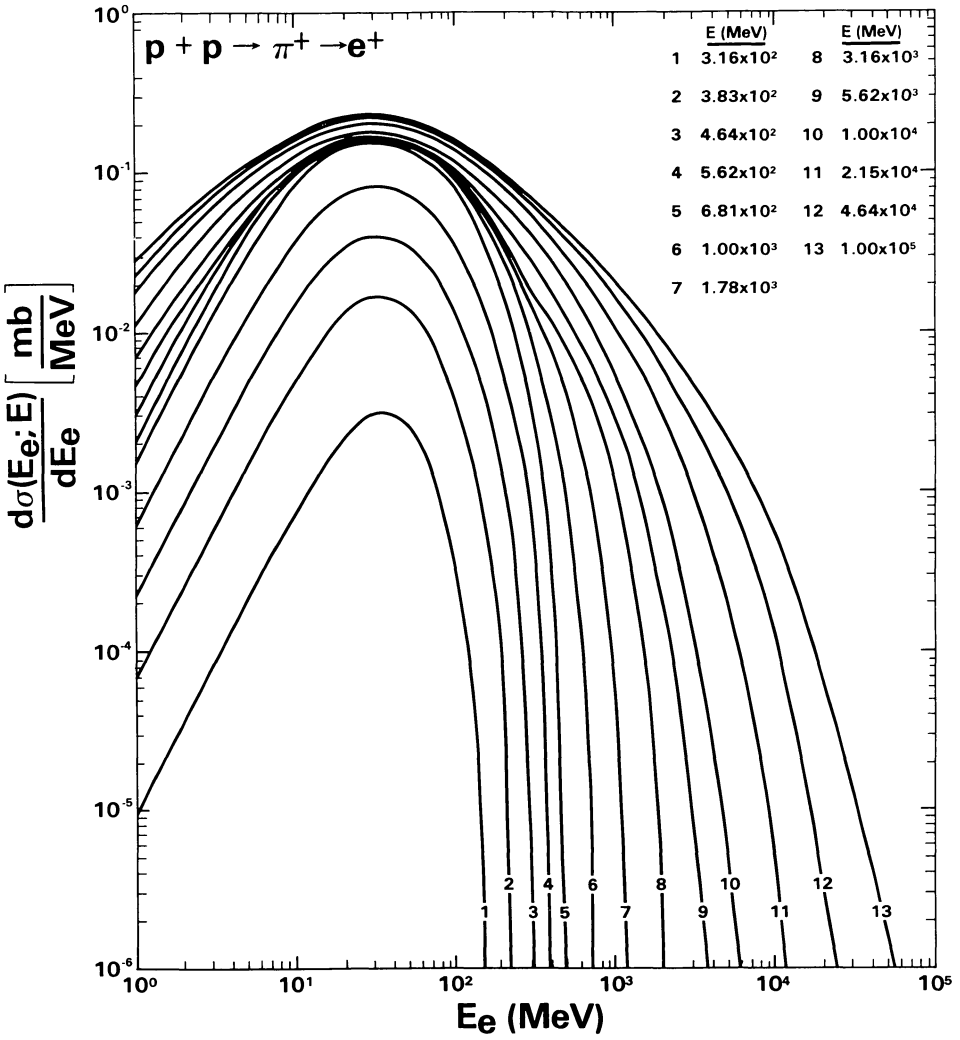

FIG. 7.—Energy spectra of positrons resulting from the decay of π^+ mesons produced in collisions of isotropic, monoenergetic protons with protons at rest, at a variety of proton kinetic energies.

estimate the correct isobar angular distribution from CMS neutron angular data, because the neutrons are directed opposite to the outgoing $\Delta^{++}_{3/2}$ resonance, and this resonance dominates secondary production in the single-isobar model. These data were fitted to the expression

$$N(\cos\theta^*; E) = A(E) + B(E)\cos^2\theta^*, \qquad (5)$$

where θ^* is the angle the isobar makes in the CMS with respect to the direction of motion of a colliding proton. The resulting spectrum, shown by the dashed histogram in Figure 9 from a Monte Carlo calculation, is now in much better agreement with the neutron data. This revised isobar distribution had negligible effect on the LS pion spectrum.

At high energies, Tan and Ng (1983) developed a scaling representation that accurately describes secondary proton production in p-p collisions. We assume that this representation also describes secondary neutron production at these energies. We have found that both the scaling representation and the isobar model successfully describe LS neutron data at 2.0 GeV, but at energies < 2 GeV the isobar model gives a better fit to the data than the scaling model (see curve 2 in Fig. 9). On the other hand, the scaling model is superior at higher energies. We therefore use the isobar model for secondary neutron and proton production at energies below 2.0 GeV and the scaling representation above 2.0 GeV, after normalizing the models to the respective neutron and proton inclusive cross sections.

b) Neutron and Proton Production in Reactions Not Involving Pions

In this section we consider in detail the production of neutrons and protons from p-p, p-α, and α-α reactions. A detailed discussion of the production of neutrons and protons in collisions involving heavier nuclei will be given elsewhere.

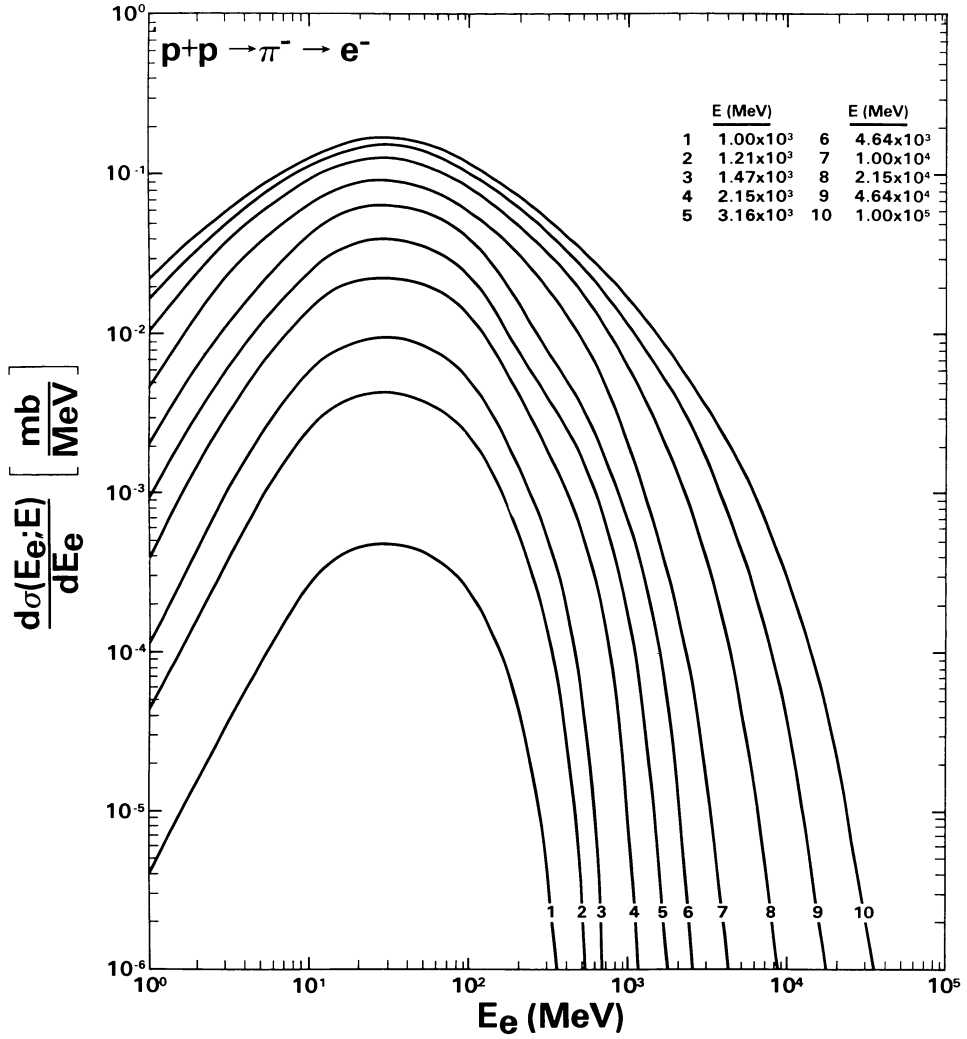

FIG. 8.—Energy spectra of electrons resulting from the decay of π^- mesons produced in collisions of isotropic, monoenergetic protons with protons at rest, at a variety of proton kinetic energies.

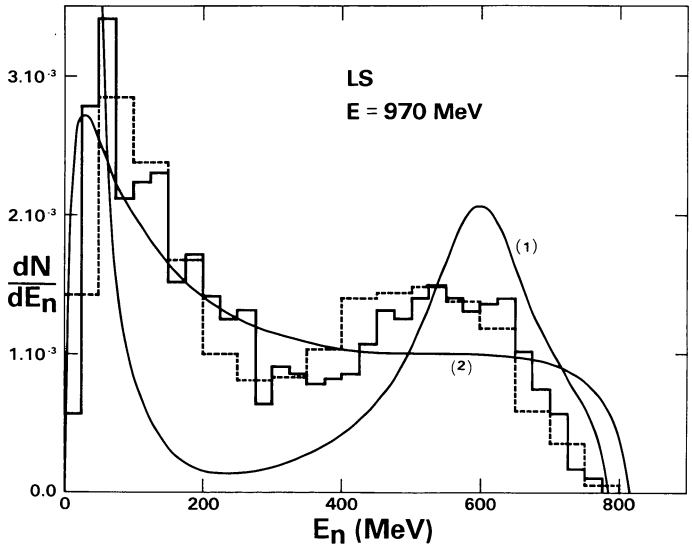

FIG. 9.—Laboratory system energy spectrum of neutrons produced in proton-proton interactions at 970 MeV. *Solid histogram*: experimental data of Bugg *et al.* (1964); *dashed histogram*: isobar model prediction with a CMS isobar angular distribution as described in the text. *Curve 1*: neutron spectrum if the isobars are assumed to travel along the directions of the incident protons in the CMS; *curve 2*: scaling model prediction of Tan and Ng (1983) for proton production in *p-p* collisions at 970 MeV.

i) *p-p and p-α Reactions*

The relevant reactions are listed in Table 3. The cross sections of these reactions, based on laboratory measurements, were summarized by Meyer (1972). The cross sections of the neutron-producing reactions 3, 4, and 5 are shown in Figure 10. The experimental CMS angular distributions for the elastic reactions 1 and 2 can also be found in the work of Meyer. We approximated the angular distributions for reaction 1 by an expression of the form of equation (5). For reaction 2, we fitted the measured distributions by an exponential in cos θ^* (see Ramaty and Lingenfelter 1969). But there are essentially no measurements of the energy and angular distributions of the secondary neutrons and protons in the multibody, inelastic reactions 3–7. For these reactions we assume an isotropic CMS angular distribution and a flat energy distribution up to a maximum obtained when the neutron or proton moves in one direction and all the other particles move in the opposite direction. Using this model, we have evaluated the LS neutron energy spectrum for reaction 3 and compared it with the measured (Tannenwald 1953) energy distribution of protons resulting from the mirror reaction $n + \alpha \rightarrow {}^3\mathrm{H} + 2p$ at 90 MeV incident neutron energy. The results are in reasonable agreement. We have also compared this model with a 3-body phase-space model (e.g., Perl 1974) for reactions 3, 6, and 7. In this model the CMS angular distribution of an outgoing particle is isotropic, and its energy distribution is proportional to the available volume in phase space. We have found that the differences between the 3-body phase-space distribution and a flat distribution are small.

TABLE 3

REACTIONS OF PROTONS AND ALPHA PARTICLES NOT INVOLVING PIONS

Reaction Number	Reaction	Reaction Number	Reaction
1	$p + p \rightarrow p + p$	5	$p + \alpha \rightarrow 3p + 2n$
2	$p + \alpha \rightarrow p + \alpha$	6	$p + \alpha \rightarrow {}^3\mathrm{H} + 2p$
3	$p + \alpha \rightarrow {}^3\mathrm{He} + p + n$	7	$p + \alpha \rightarrow 2({}^2\mathrm{H}) + p$
4	$p + \alpha \rightarrow {}^2\mathrm{H} + 2p + n$		

ii) *α-α Reactions*

The inclusive neutron production cross section in α-α reactions is shown in Figure 10. The cross sections for the fusion reactions $\alpha + \alpha \rightarrow {}^7\mathrm{Be} + n$ and $\alpha + \alpha \rightarrow {}^6\mathrm{Li} + p + n$ were summarized by Ramaty, Kozlovsky, and Lingenfelter (1979). Near the α-α inelastic threshold (9.5 MeV nucleon^{-1}), we assume that these two reactions are the dominant channels. Above ~12 MeV nucleon^{-1}, the cross sections of these two channels decrease (Glagola *et al.* 1982). The next important inelastic reactions involve the breakup of one alpha particle in the field of the other (analogous to the breakup of α in *p*-α reactions); e.g., $\alpha + \alpha \rightarrow \alpha + {}^3\mathrm{He} + n$, $\alpha + \alpha \rightarrow \alpha + {}^3\mathrm{H} + p$, $\alpha + \alpha \rightarrow \alpha + {}^2\mathrm{H} + p + n$, $\alpha + \alpha \rightarrow \alpha + 2p + 2n$. Channels with higher energy thresholds involve the breakup of both alpha particles. Paic *et al.* (1981) measured the inclusive proton differential cross sections for α-α reactions. We numerically integrated the Paic results at 27.5, 32.5, 39.6, and 43 MeV nucleon^{-1} and, because of the symmetry between protons and neutrons in α-α reactions, assume that the inclusive proton and neutron cross sections are identical. At higher energies, we assume that the cross sections approach a constant value (see Fig. 10).

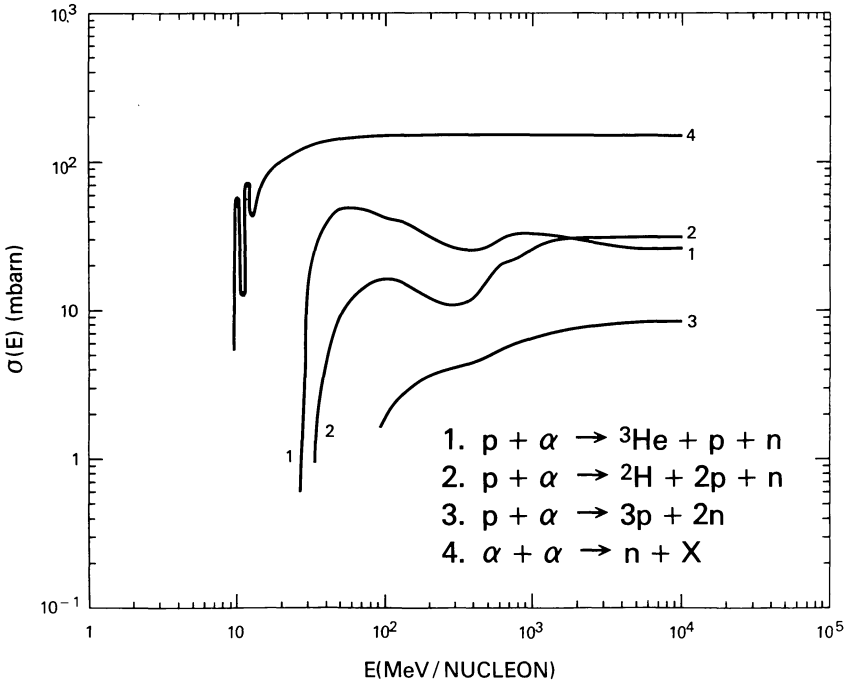

FIG. 10.—Cross sections for neutron production, including the neutron multiplicity, in reactions of protons and alpha particles with alpha particles

We used equation (5) to fit the angular data (Glagola *et al.* 1982) of the two fusion reactions. We then assumed that this distribution also represents the secondary proton and neutron angular distributions in the other α-α reactions. For the energy distributions, we used a flat distribution up to a maximum value attained when all other particles recoil in a direction opposite to that of the proton or neutron, as in the p-α reactions. This allows the neutron to attain a very high energy. The resultant distribution in the LS was not found to be very sensitive to details of the angular assumptions in the CMS at high energies.

IV. BREMSSTRAHLUNG AND ANNIHILATION IN FLIGHT

In this section we derive expressions for the production of bremsstrahlung and broad-band annihilation radiation from positrons and electrons of an arbitrary spectrum in a thick target, taking into account Coulomb, bremsstrahlung, and synchrotron losses, as well as the removal of the positrons by annihilation in flight.

Detailed calculations of the instantaneous bremsstrahlung production by electrons with power-law energy distributions and various angular distributions were carried out recently by Dermer and Ramaty (1986), using accurate e-p and e-e bremsstrahlung cross sections which are valid over a broad energy range. These calculations, however, are not directly applicable here because the spectra of the secondary positrons and electrons differ from power laws and the calculations were not extended to the thick-target case. We have derived an approximate thick-target formula for the calculation of bremsstrahlung from monoenergetic and isotropic positrons and electrons, taking into account Coulomb, bremsstrahlung, and synchrotron losses and positron annihilation in flight. This formula is valid in the photon energy range from ~ 10 to 300 MeV. When simplified to the thin-target case and integrated over a power law, it is in good agreement with the isotropic calculations of Dermer and Ramaty (1986). This formula can be integrated numerically over the secondary positron and electron spectra which are derived in § V, as well as over primary electron spectra.

The total energy loss rate due to Coulomb interactions, bremsstrahlung, and synchrotron radiation can be written as

$$\left(\frac{dE_e}{dt}\right)_{\rm tot} = 1.14 m_p n_{\rm H} c\left[\left(\frac{dE_e}{dx_{\rm H}}\right)_{\rm Coul} + \left(\frac{dE_e}{dx_{\rm H}}\right)_{\rm brem}\right] + \left(\frac{dE_e}{dt}\right)_{\rm sync} ({\rm MeV\ s^{-1}}), \quad (6)$$

where $(dE_e/dx_{\rm H})_{\rm Coul} \approx 3.90 E_e^{0.06}$ MeV (g cm^{-2})$^{-1}$ (valid from ~ 10 to 500 MeV; Berger and Seltzer 1964), $(dE_e/dx_{\rm H})_{\rm brem} \approx 6.56\times10^{-3} E_e^{1.14}$ MeV (g cm^{-2})$^{-1}$ (also valid from ~ 10 to 500 MeV; Berger and Seltzer 1964), $(dE_e/dt)_{\rm sync} = 3.75\times10^{-9} B_\perp^2 E_e^2$ MeV s^{-1} (Ginzburg and Syrovatskii 1964), $n_{\rm H}$ is the ambient hydrogen density in cm^{-3}, $B_\perp$ is the average perpendicular component of the magnetic field in gauss, and the factor 1.14 takes into account the effects of the ambient helium for $n_{\rm He}/n_{\rm H} = 0.07$. In addition to losing energy, the positrons can also annihilate in flight. The probability of survival against annihilation while slowing down from E_0 to E_e is given by

$$P(E_0, E_e) = \exp\left[-1.14 n_{\rm H} c \int_{E_e}^{E_0} dE_e' \frac{\sigma_a(E_e')}{(dE_e'/dt)_{\rm tot}}\right], \quad (7)$$

where $\sigma_a(E_e)$ is the positron-electron annihilation cross section and the factor 1.14 takes into account the effects of helium. For ultrarelativistic positrons, $\sigma_a(E_e) = 1.27\times 10^{-25}[\ln(3.91E_e) - 1]/E_e$ cm^2, where E_e is in MeV (Heitler 1957). We have evaluated equation (7) numerically, and the results for $E_e = 2$ MeV are shown in Figure 11 for various values of $B_\perp$. This probability is essentially the survival probability to reach the energy at which the 0.511 MeV line is formed (less than 1 keV) because the probability of annihilating in flight below 2 MeV is very small. The survival probability between any two energies on the abscissa in Figure 11 is the ratio between the survival probabilities to 2 MeV at the two energies. As can be seen, the effect of a magnetic field is to decrease the probability for annihilation in flight at high energies.

The thick-target bremsstrahlung production from monoenergetic positrons or electrons with initial energy E_0 is given by

$$\frac{dQ_B}{d\varepsilon}(E_0, \varepsilon) = \frac{1}{\varepsilon}\int_\varepsilon^{E_0} \frac{dE_e}{E_e} \frac{(dE_e/dt)_{\rm brem}}{(dE_e/dt)_{\rm tot}} P(E_0, E_e)\ ({\rm MeV^{-1}}), \quad (8)$$

where we have approximated the bremsstrahlung energy spectrum from a single positron or electron by a flat distribution in the range $0 \le \varepsilon \le E_e$. By substituting the above expressions for $(dE_e/dt)_{\rm brem}$ and $(dE_e/dt)_{\rm tot}$ and by approximating P with a constant, we obtain

$$\frac{dQ_B}{d\varepsilon}(E_0, \varepsilon) = 6.56\times10^{-3}\frac{P}{\varepsilon} \times \int_\varepsilon^{E_0} \frac{dE_e}{3.90E_e^{-0.08} + 6.56\times10^{-3}E_e + 6.57\times10^4 E_e^{1.86} B_\perp^2/n_{\rm H}} \quad (9)$$

in MeV^{-1} with $P = 1.0$ for electrons, and we take $P = 0.9$ for positrons. To evaluate equation (9) analytically, we have approximated the denominator inside the integral by $a + bE_e + cE_e^2$, where $a = 3.10$, $b = 5.20\times10^{-3}$, and $c = 2.70\times 10^4 B_\perp^2/n_{\rm H}$. In the electron energy range ~ 10 to 500 MeV and $B_\perp^2/n_{\rm H} < 9\times10^{-9}$ G^2 cm^3, these two expressions differ by no more than 7%. (For $n_{\rm H} = 10^{13}$ cm^{-3}, this corresponds to $B_\perp < 300$ G.) Performing the integration, we obtain

$$dQ_B(E_0, \varepsilon)/d\varepsilon = 6.56\times10^{-3}(P/\varepsilon) \times \left[f(E_0, B_\perp^2/n_{\rm H}) - f(\varepsilon, B_\perp^2/n_{\rm H})\right], \quad (10)$$

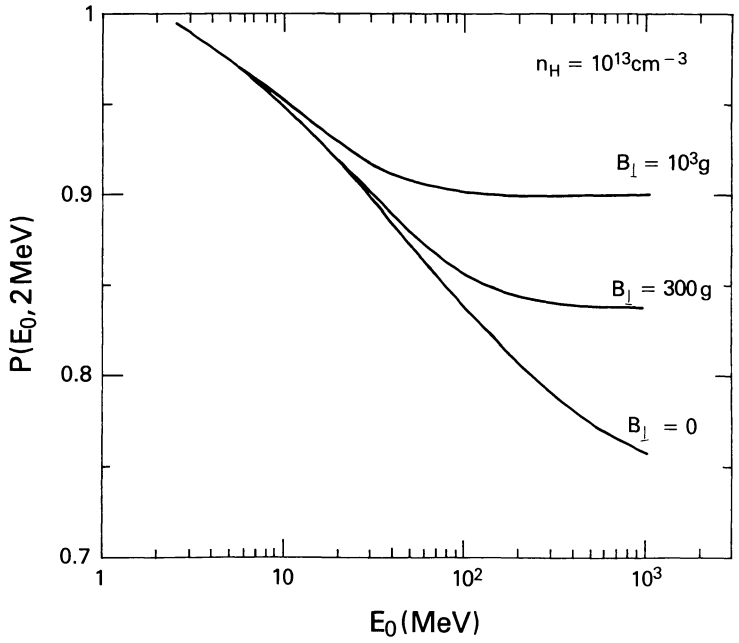

FIG. 11.—Probability that a positron with initial energy E_0 will survive to energy $E_e = 2$ MeV without annihilating for various values of the magnetic field.

where

$$f(E, B_\perp^2/n_H) = \begin{cases} 2q^{-1/2} \arctan[(2cE+b)/\sqrt{q}], & q>0, \\ (-q)^{-1/2} \ln\{[2cE+b-\sqrt{(-q)}] \\ \quad /[2cE+b+\sqrt{(-q)}]\}, & q<0, \end{cases} \tag{11}$$

and $q = 4ac - b^2$.

To check the simplified bremsstrahlung spectrum that we use, we derive the instantaneous (i.e., thin-target) bremsstrahlung rate in hydrogen produced by isotropic electrons with a power-law spectrum, $U(E_e) = n_0(s-1)(0.511)^{s-1}E_e^{-s}$ (electrons MeV^{-1} cm^{-3}) and compare the results with the isotropic calculations of Dermer and Ramaty (1986). We obtain

$$\frac{dQ_B}{d\varepsilon}(\varepsilon) = \frac{1}{4\pi\varepsilon}\int_\varepsilon^\infty \frac{dE_e}{E_e} U(E_e)\left(\frac{dE_e}{dt}\right)_{\rm H,brem}$$

$$(\text{photons cm}^{-3}\ \text{s}^{-1}\ \text{MeV}^{-1}\ \text{sr}^{-1}), \tag{12}$$

which yields $[dQ_B(\varepsilon)/d\varepsilon](\varepsilon/0.511)^s = 5.23\times10^{-17} n_H n_0 \varepsilon^{0.14}(s-1)/(s-1.14)$ (photons cm^{-3} s^{-1} MeV^{-1} sr^{-1}). In the energy range ~10–100 MeV and $s = 2.5$ or 3.5, this expression agrees with the results of Dermer and Ramaty (1986) to better than 10%.

To calculate the photon spectrum resulting from positron annihilation in flight, we make use of the fact that, for ultrarelativistic positrons, one of the annihilation photons takes up essentially all of the positron energy, while the other is emitted at $\sim m_e c^2$. Since many more positrons annihilate near rest than in flight, we can ignore the latter. The thick-target spectrum resulting from a positron of initial energy E_0 can then be written as

$$\frac{dQ_a}{d\varepsilon}(E_0, \varepsilon) = 1.14 n_H c \times \int_0^{E_0} dE_e\, \sigma_a(E_e) \frac{\delta(E_e-\varepsilon)}{(dE_e/dt)_{\rm tot}} P(E_0, E_e)\ (\text{MeV}^{-1}), \tag{13}$$

where, as before, the factor of 1.14 takes into account the effects of helium. Substituting the above expressions for σ_a and $(dE_e/dt)_{\rm tot}$ and setting $P = 0.9$, we obtain

$$\frac{dQ_a}{d\varepsilon}(E_0, \varepsilon) = \frac{0.068}{\varepsilon} \times \frac{\ln(3.91\varepsilon)-1}{3.90\varepsilon^{0.06} + 6.56\times10^{-3}\varepsilon^{1.14} + 6.57\times10^4 \varepsilon^2 B_\perp^2/n_H}\ (\text{MeV}^{-1}) \tag{14}$$

for $\varepsilon < E_0$ and $dQ_a/d\varepsilon = 0$ for $\varepsilon \geq E_0$.

The thick-target bremsstrahlung, $dQ_B/d\varepsilon$, or the broad-band annihilation radiation, $dQ_a/d\varepsilon$, produced by a distribution of positrons or electrons is then given by

$$\frac{dQ_{B,a}}{d\varepsilon}(\varepsilon) = \int_0^\infty dE_e\, N_e(E_e) \frac{dQ_{B,a}}{d\varepsilon}(E_e, \varepsilon)\ (\text{MeV}^{-1}), \tag{15}$$

where $N_e(E_e)$ is the number of positrons or electrons injected into the interaction region per unit energy.

V. NUMERICAL RESULTS

We now present the results of numerical calculations of secondary proton, neutron, and gamma-ray production using the stochastic-acceleration and shock-acceleration spectra, equations (1) and (2), respectively. We carry out calculations with various value of αT, s, and E_{0p}, and evaluate the E_{0i} from equation (3). We normalize these spectra in such a way that the number of protons with energy greater than 30 MeV, $N_p(>30$ MeV), is unity, and we choose the abundance parameters C_i proportional to either the ambient medium composition or the 1982 June 3 composition (see Table 1). In several calculations, we single out the values $\alpha T = 0.04$ and $s = 2.4$, since these provide good fits to the June 3 data, which we discuss in detail in § VI (see also § II). We carry out our calculations in the thick-target model (§ II). Thus, the $N_i(>E)$ are the total numbers of particles of species i with energy (or energy per nucleon) greater than E incident on the interaction region in a specified time period (the duration of the flare or a fraction thereof). We denote the differential yields (per unit energy or energy per nucleon) produced in this time period by dQ/dE for particles and $dQ/d\varepsilon$ for photons. We emphasize again that in the transrelativistic region, equation (1) is not a valid solution of the stochastic-acceleration transport equation. Consequently, this equation should be considered only as a convenient mathematical expression in calculations at high energies.

a) Proton Production

We have evaluated the production of protons in p-p, p-α, α-p, and α-α reactions using the cross sections and distributions described in § III. Results for shock-acceleration spectra with $s = 2.4$, $E_{0p} = 1000$ and 3000 MeV, and C_i proportional to the ambient medium composition are shown in Figure 12. The secondary proton spectra shown result from interactions

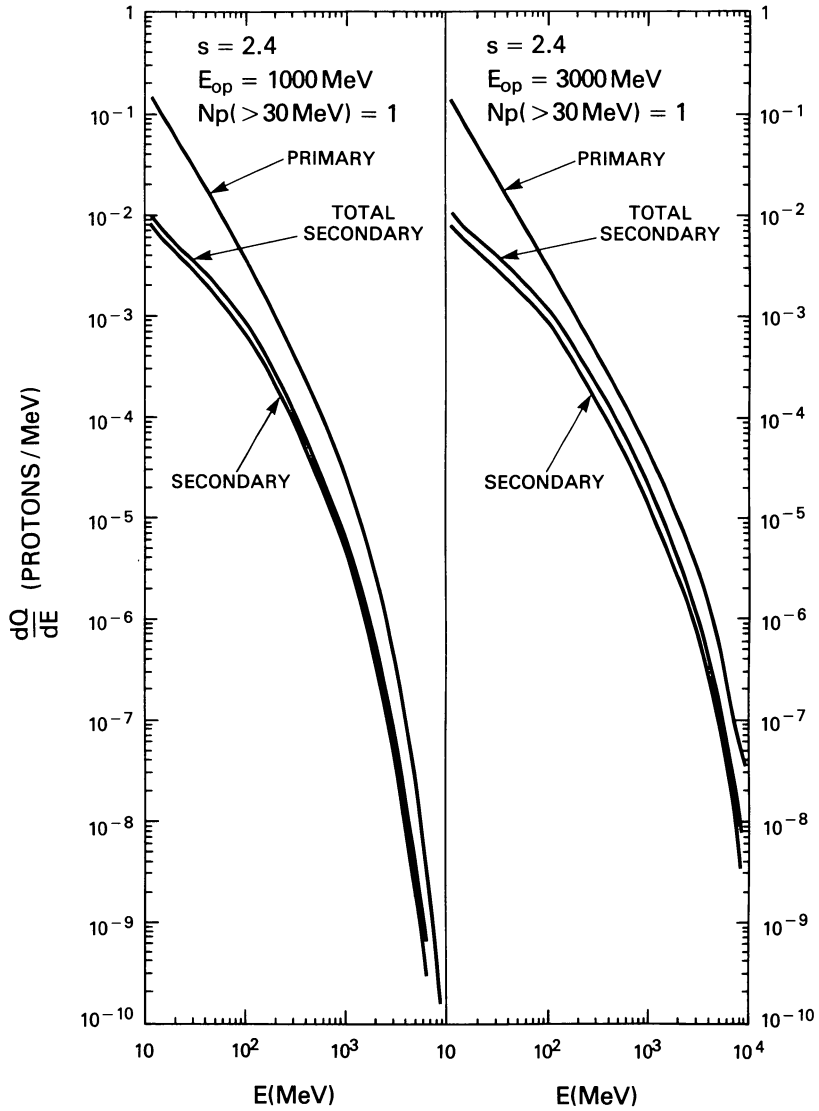

FIG. 12.—Primary shock-acceleration proton spectra and first-generation secondary and total secondary proton spectra resulting from interactions of the primary protons with the ambient medium.

of just the primary spectra. We have also calculated the secondary proton spectra resulting from these first-generation secondaries and continued the process until it converged (two and three iterations were sufficient for $E_{0p} = 1000$ and 3000 MeV, respectively). The resultant total secondary spectra are also shown. By comparing these total secondaries with the primaries, we see that the secondary proton spectra are at most $\sim 30\%$ and $\sim 50\%$ of their respective associated primary spectra. Carrying out similar calculations for primary proton spectra given by stochastic-acceleration spectra, we find that for $\alpha T \lesssim 0.07$ the secondary proton spectra are even less important. For the June 3 flare (which has the hardest proton spectrum of all the gamma-ray–producing flares observed so far; see Murphy and Ramaty 1985), E_{0p} is expected to be less than 1000 MeV and $\alpha T \approx 0.04$ (§ VI). Thus, we do not expect secondary protons to be of great importance in flares, and we neglect them in our subsequent calculations. The calculated values of the total number of interacting particles are too high by about 30%, but the errors in the ratios of the various radiation fluxes are much smaller.

b) *Neutron Production*

We have evaluated the production of neutrons in p-p, p-α, α-p, and α-α reactions using the cross sections and distributions described in § III. We have also incorporated the interactions of protons and alpha particles with nuclei heavier than helium, whose cross sections and distributions will be described in detail elsewhere. The resultant neutron production spectra are shown in Figure 13 for various values of αT and s with $E_{0p} = 3000$ MeV and C_i proportional to the ambient medium composition. Partial and total neutron production spectra are shown by the solid curves in Figures 14 and 15 for a stochastic-acceleration spectrum with $\alpha T = 0.04$ and a shock-acceleration spectrum with $s = 2.4$ and $E_{0p} = 1000$ MeV, respectively, and C_i proportional to the ambient medium composition in both cases. The dashed curves in these figures represent the total neutron production spectrum for C_i proportional to the June 3 composition. The curves labeled p, α, CNO, and Ne–Fe represent, respectively, neutron spectra from energetic protons, alpha particles, C, N, and O nuclei, and nuclei from Ne through Fe interacting with the ambient medium.

For the stochastic-acceleration spectrum (Fig. 14), below ~ 10 MeV the bulk of the neutrons are produced by accelerated protons (mostly via p-α reactions), while at higher energies the bulk of the production is due to fast alpha particles (mostly via α-p and α-α reactions). Neutron production in this case is very sensitive to the energetic particle composition, as can be seen by comparing the total solid and dashed curves. We note that the reduction in neutron production is due almost entirely to the reduction of the alpha-particle abundance relative to that of the protons (see Table 1). For the shock-acceleration spectrum (Fig. 15), the bulk of the

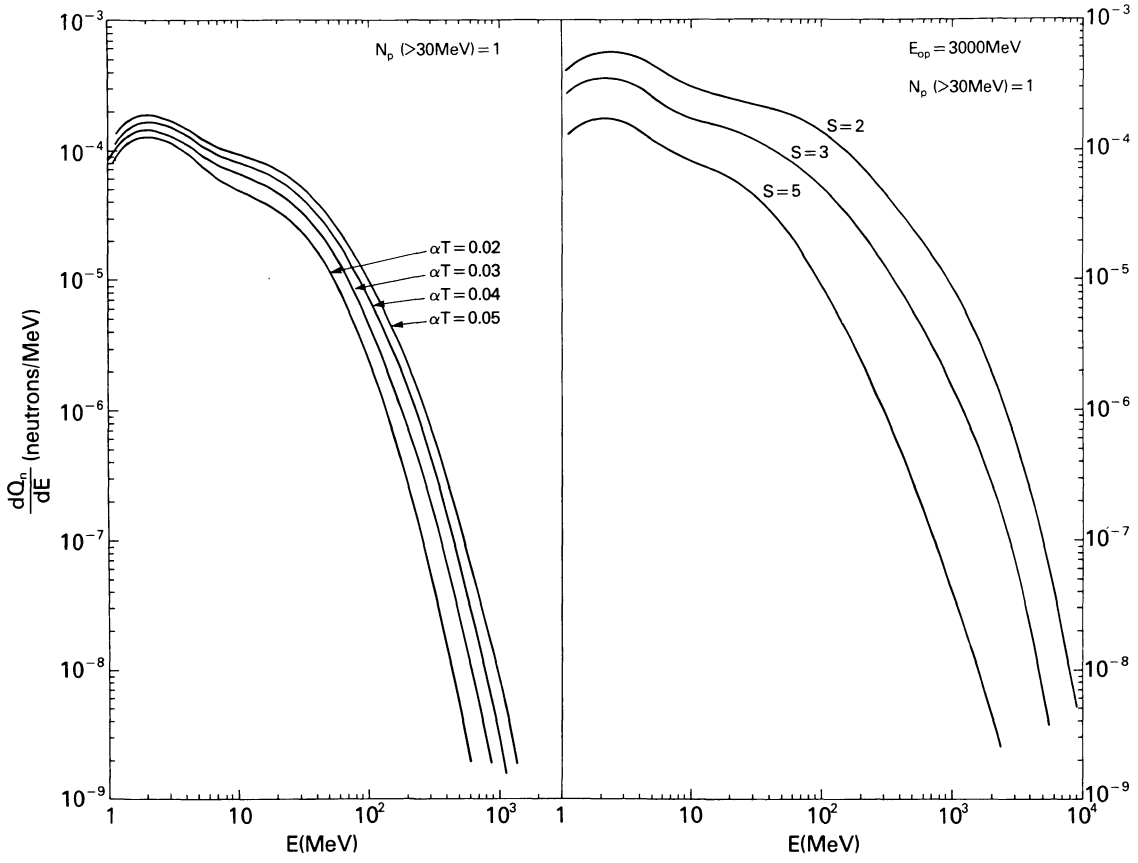

FIG. 13.—Total neutron production spectra for a variety of primary energetic-particle spectra, and ambient composition for the particles (Table 1)

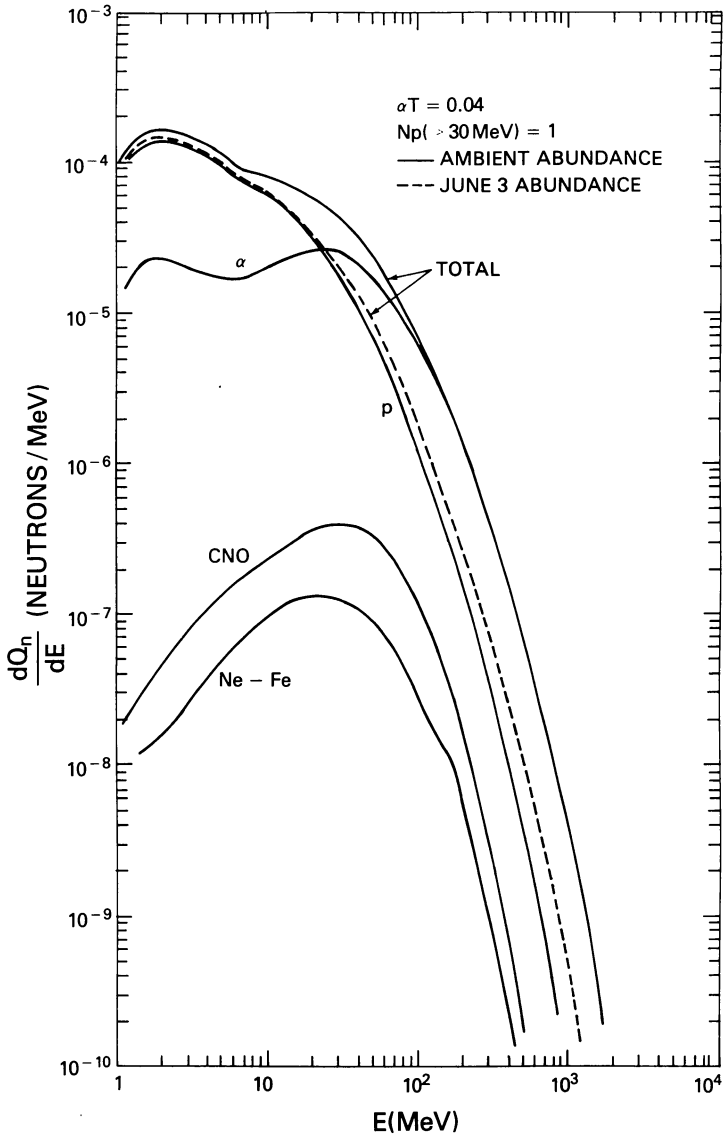

FIG. 14.—Partial neutron production spectra for a primary stochastic-acceleration spectrum with $\alpha T = 0.04$ and ambient composition. The total neutron production spectrum for a primary composition given by the June 3 composition (Table 1) is shown by the dashed curve. Curves labeled p, α, CNO, and Ne-Fe represent, respectively, neutron spectra from energetic protons; alpha particles; C, N, and O nuclei; and nuclei from Ne through Fe interacting with the ambient medium.

neutrons are produced by accelerated protons, mostly via p-α reactions at low energies and p-p reactions at high energies. In this case the total neutron spectrum is not so sensitive to the α/p ratio.

c) *Gamma-Ray Production from Pions*

We have evaluated the production of positrons and electrons from charged π decay and the production of gamma rays from π^0 decay using the cross sections and distributions described in § III. The production spectra of positrons and electrons for shock-acceleration spectra with $s = 2.4$, $E_{0p} =$ 1000 and 3000 MeV, and C_i proportional to the ambient medium composition are shown in Figure 16. Using such positron and electron spectra and the formulae of § IV, we have evaluated the bremsstrahlung and the gamma-ray emission from positron annihilation in flight. Results for a stochastic-acceleration spectrum with $\alpha T = 0.04$ and for a shock-acceleration spectrum with $s = 2.4$ and $E_{0p} = 1000$ MeV are shown by the solid curves in Figures 17 and 18, respectively, for C_i proportional to the ambient medium composition and $B_\perp = 0$ in both cases. As can be seen, above a few tens of MeV, radiation from π^0 decay dominates, while at lower energies radiation from positrons is most important. The dashed curves in these figures represent the total radiation from pions for the 1982 June 3 composition. We note that the variation with composition is not so pronounced here as in the case of neutron production.

We have also plotted in Figures 17 and 18 the nuclear de-excitation spectra using the cross sections and techniques

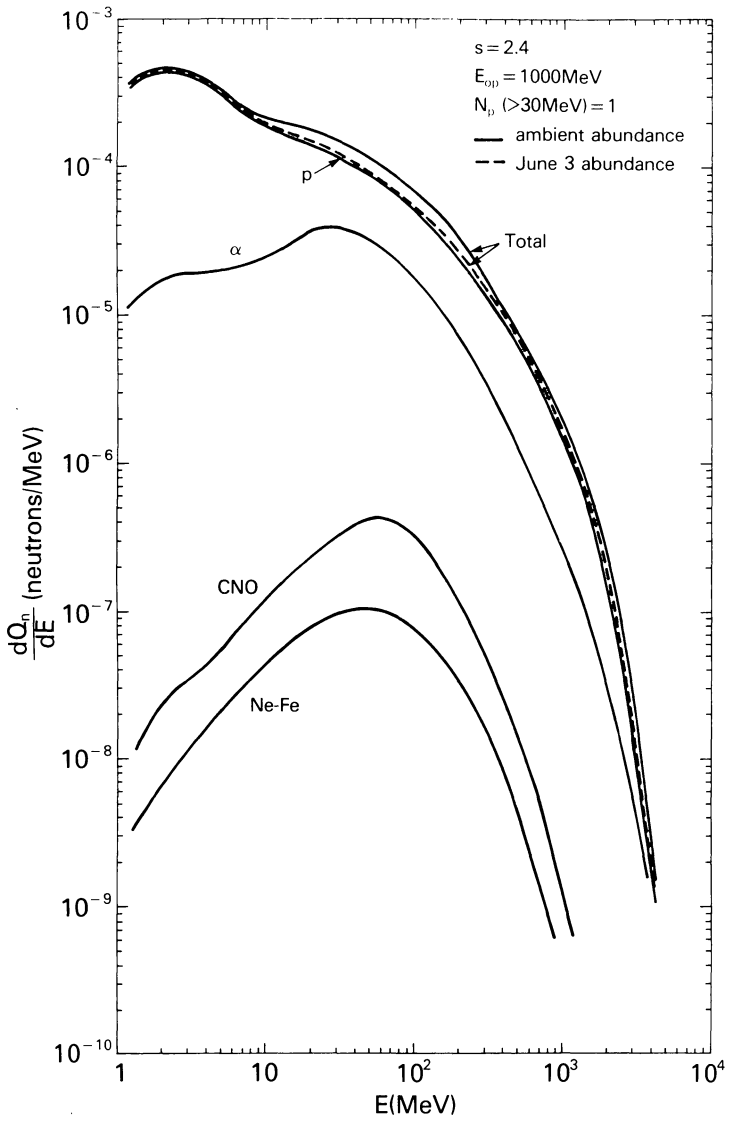

FIG. 15.—Same as Fig. 14, but for a primary shock-acceleration spectrum with $s = 2.4$ and $E_{0p} = 1000$ MeV

described by Ramaty, Kozlovsky, and Lingenfelter (1979), Murphy *et al.* (1985*a*), and Murphy (1985). While the widths of many nuclear lines are quite narrow, we have used a bin width of 1 MeV appropriate to the degraded energy resolution of the *SMM* detector during intense, impulsive flares. During more gradual flares, the *SMM* detector is capable of better resolution, as for example the flare of 1981 April 27 (Murphy *et al.* 1985*b*). The ratio of nuclear de-excitation flux to the total pion-decay flux is a strong function of the spectrum of the primary protons, as can be seen by comparing Figures 17 and 18. This effect is shown for a broader range of parameters in Figure 19, where we plot the ratio of the total differential pion-decay radiation at 100 MeV for $B_\perp = 0$ to the integrated nuclear line emission between 4.1 and 6.4 MeV as functions of αT and E_{0p} (with $s = 2.4$). The solid and dashed curves are for C_i proportional to the ambient medium and June 3 compositions, respectively.

The effect of synchrotron losses is shown in Figure 20 for gamma-ray spectra from pion decay and from primary electron bremsstrahlung. The pion production has been calculated for a shock-acceleration spectrum with $s = 2.4$, $E_{0p} = 1000$ MeV, and C_i proportional to the ambient medium composition. Note that as $B_\perp^2 / n_H$ increases, the contribution of secondary positrons and electrons to the broad-band gamma-ray production decreases, while the contribution of the neutral pions remains the same. The primary electron spectrum has the same value of s as the protons, a value of E_{0e} deduced from equation (3) with $E_{0p} = 1000$ MeV, and is normalized in such a way that the accelerated electron and proton fluxes are equal at ~ 3 MeV (see Fig. 2). Thus, for an e/p ratio and the hard proton spectrum implied by the June 3 observations, the secondary positrons and electrons resulting from thick-target interactions produce more gamma rays than the primary electrons.

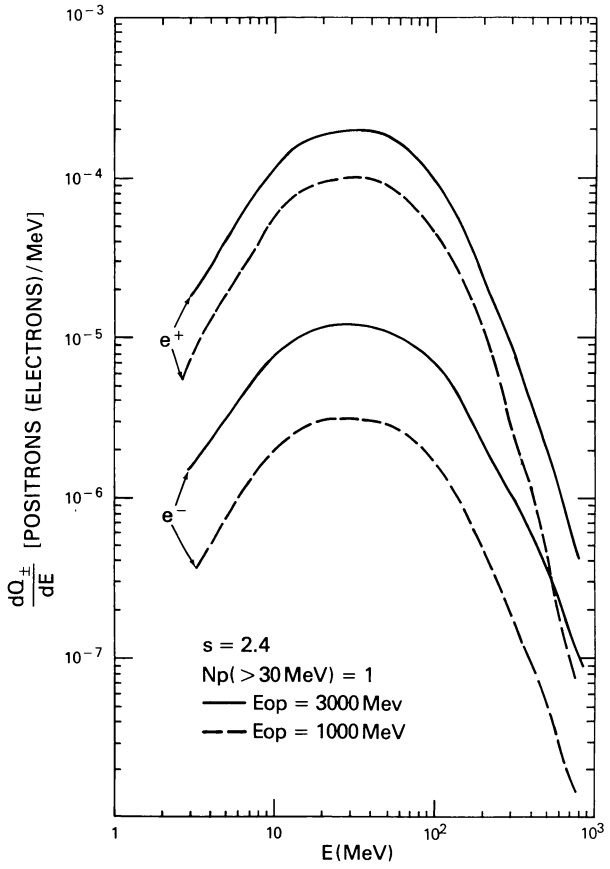

FIG. 16.—Production spectra of positrons and electrons for primary shock-acceleration spectra, and ambient abundance for the energetic particles.

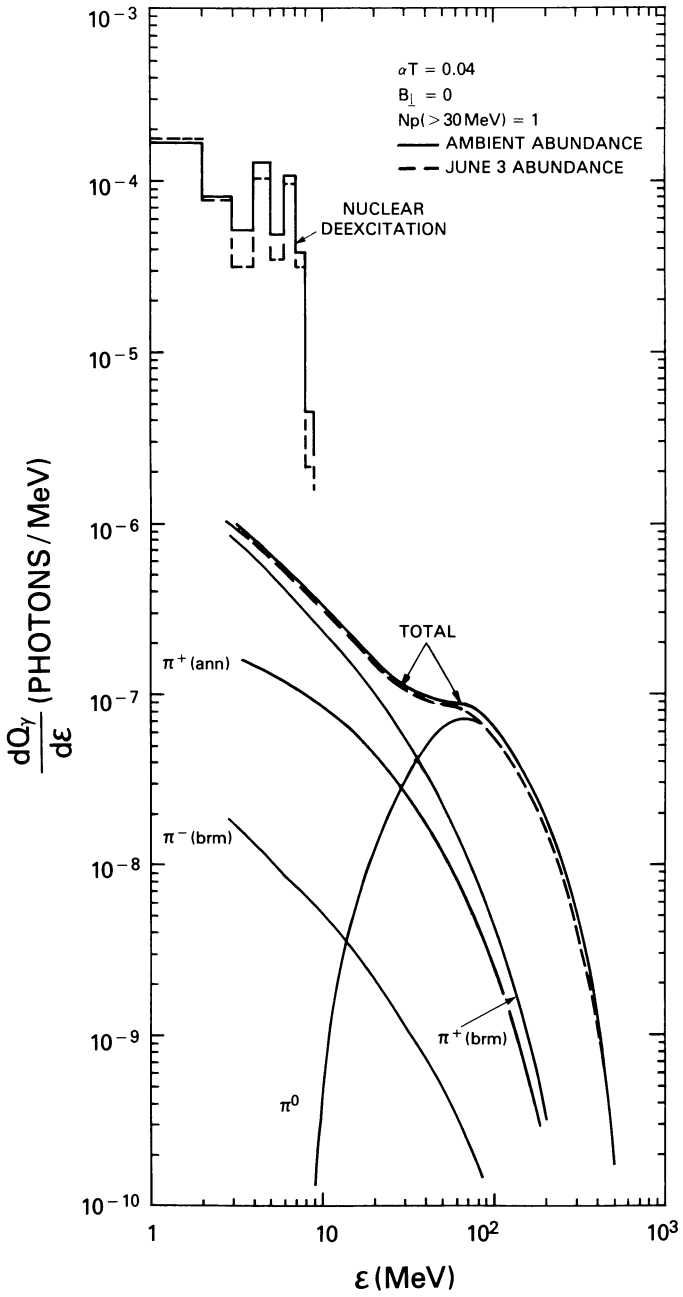

FIG. 17.—Gamma-ray spectrum resulting from pion production and nuclear de-excitation for a primary stochastic-acceleration spectrum with $\alpha T = 0.04$ and ambient composition. The total gamma-ray spectrum for a primary composition given by the June 3 composition (Table 1) is shown by the dashed curve and the histogram.

Gamma rays from π^0 decay are prompt, since the lifetime of the neutral pion is very short. The timing of the gamma rays from bremsstrahlung and annihilation in flight of the secondary positrons and electrons depends on the density and magnetic field. For $B_{\perp} = 0$ and a photon energy around 30 MeV, the delay between the production of the charged pions and the release of the gamma rays is approximately 3×10^{14} s/$n_{\rm H}$(cm^{-3}). For a finite $B_{\perp}$ this delay is shorter.

d) *Line Production from Positron Annihilation, Neutron Capture and Nuclear De-excitation*

Positrons resulting from the decay of both π^+ mesons and radioactive beta emitters contribute to the 0.511 MeV line. The production of beta emitters for stochastic-acceleration spectra and ambient medium compositions was calculated by Ramaty *et al.* (1983*a*) and Murphy and Ramaty (1985). Here we have performed additional calculations for shock-acceleration spectra and the June 3 composition. For positrons from π^+ decay, the average probability to survive annihilation in flight is ~ 0.8 (see Figs. 11 and 16), while for positrons from radioactive beta emitters this probability is essentially unity. The curves Q_+ (stop) in Figure 21 show the total yields of positrons that survive annihilation in flight obtained for stochastic- and shock-acceleration spectra and ambient medium and June 3 abundances. The 0.511 MeV line yield can be obtained from these surviving positron yields if the fraction of positrons annihilating from bound states of positronium is known. For annihilation in an essentially neutral medium, the 0.511 MeV photon-to-positron ratio is ~ 0.65 (Brown *et al.* 1984).

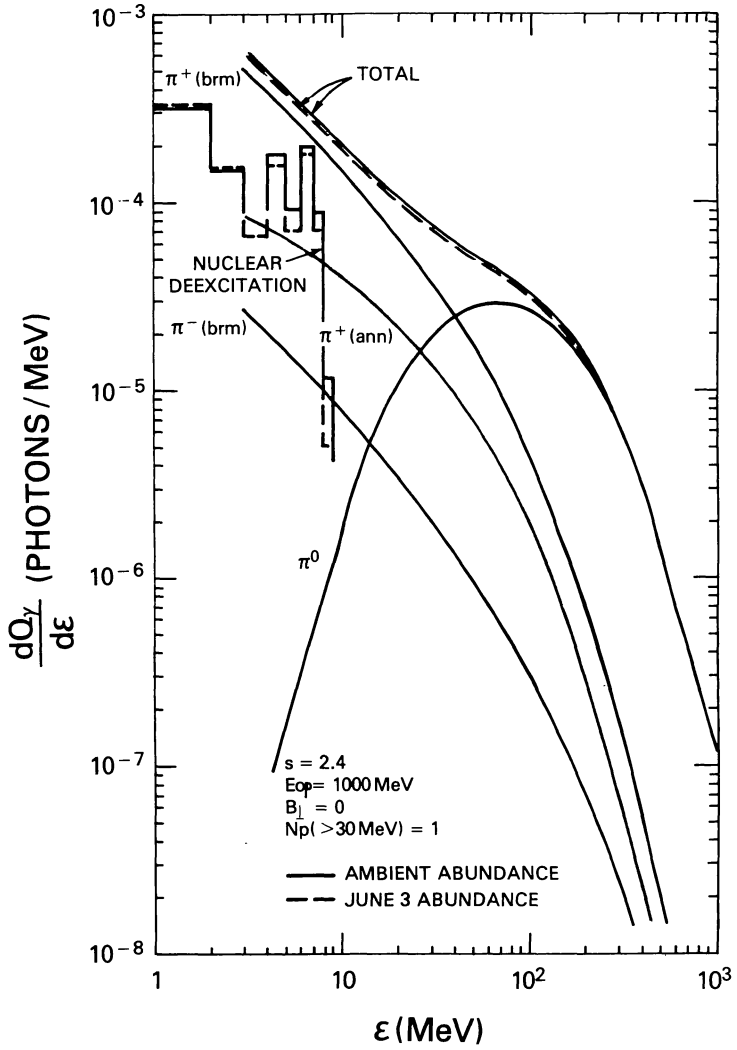

FIG. 18.—Same as Fig. 17, but for a primary shock-acceleration spectrum with $s = 2.4$ and $E_{0p} = 1000$ MeV

The production of neutrons for stochastic-acceleration spectra and ambient medium composition was also calculated by Ramaty *et al.* (1983*a*) and Murphy and Ramaty (1985). In Figure 21 we show neutron yields for both stochastic- and shock-acceleration spectra and ambient and June 3 abundances. Neutron–to–2.223 MeV photon conversion factors for stochastic-acceleration spectra were given by Murphy and Ramaty (1985). In Figure 21 we show such conversion factors for shock-acceleration spectra and ambient medium and June 3 abundances. These conversion factors are for isotropic neutron production above the photosphere.

Nuclear de-excitation lines produce a very significant excess above the continuum in the photon energy range from about 4 to 7 MeV (e.g., Ramaty 1986). Because of experimental considerations of the *SMM*/GRS instrument, this excess is observed (e.g., Forrest 1983) in the energy range from 4.1 to 6.4 MeV. The production of nuclear lines in the 4–7 MeV range was calculated by Ramaty *et al.* (1983*a*) and Murphy and Ramaty (1985) for stochastic-acceleration spectra and ambient medium composition. In Figure 21 we present calculations of the 4.1–6.4 MeV nuclear line production for both stochastic- and shock-acceleration spectra and ambient medium and June 3 compositions. The ratio of the 4.1–6.4 MeV yield to the 4–7 MeV yield depends weakly on the particle spectrum and composition, and is approximately 0.85.

Also shown in Figure 21 is the differential pion-decay radiation at 100 MeV for stochastic- and shock-acceleration spectra and ambient medium and June 3 compositions. The ratio of this differential emission to the 4.1–6.4 MeV emission was presented in Figure 19.

For $B_\perp = 0$, the time delay between the production of the π^+ mesons and the release of the 0.511 MeV photons is $\sim 3\times10^{14}$ s/n_H(cm^{-3}). The delay between the decay of a beta emitter and the production of the annihilation photon is approximately 2×10^{12} s/n_H(cm^{-3}) (see Ramaty 1986).

VI. GAMMA RAYS AND NEUTRONS FROM THE 1982 JUNE 3 FLARE

In this section we develop a self-consistent interaction model capable of accounting for all of the neutron and

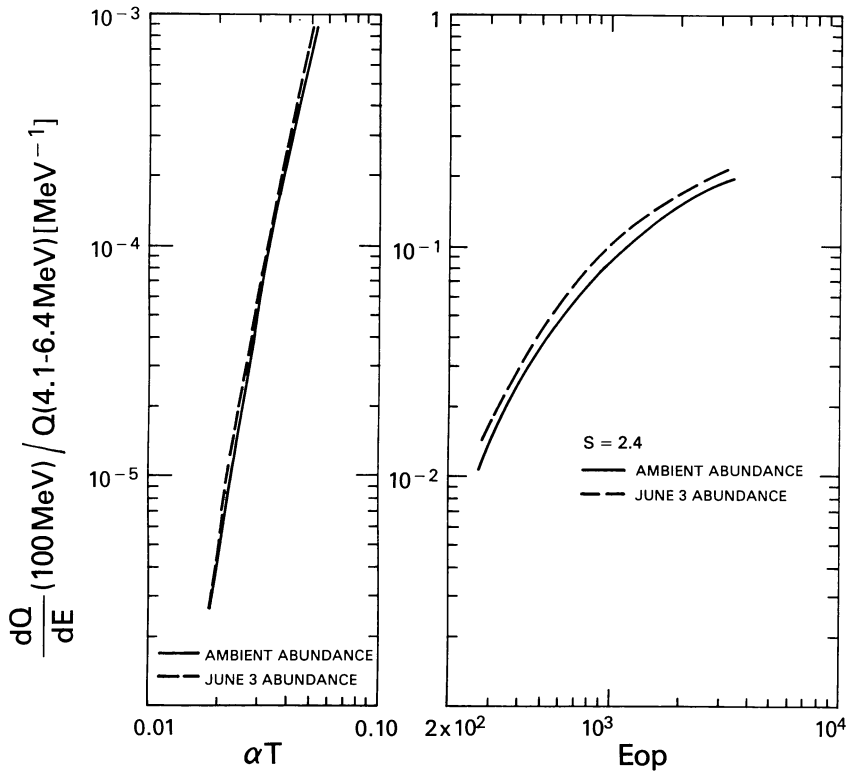

FIG. 19.—Ratio of the differential pion-decay radiation at 100 MeV to the 4.1–6.4 MeV nuclear emission for stochastic and shock-acceleration spectra

gamma-ray observations of the 1982 June 3 flare. The key ingredients are two distinct energetic particle populations having different interaction time histories and different energy spectra. Using the time-dependent observations of the >10 MeV broad-band emission, the 0.511 MeV line, and the 4.1–6.4 MeV nuclear excess, we derive the parameters of these distributions. We then show that the results are consistent with the neutron and 2.223 MeV line data. We identify the origins of the two populations in first- and second-phase acceleration and show that the particles observed in interplanetary space probably result from acceleration in the second phase. We also discuss the observations of the 1980 June 21 flare which are consistent with acceleration in a single phase.

a) Observations

We start with the June 3 gamma-ray emission above 10 MeV (Forrest *et al.* 1985) shown by the closed symbols in Figures 22 and 23 for two observation periods (11:42:44–11:43:49 UT) and (11:46:00–11:47:06 UT). Emission above 10 MeV was reported for a third period (11:47:06–11:48:11 UT), but because these data are contaminated by neutrons (Forrest *et al.* 1985), we do not consider them here. The flattening above ~ 70 MeV in Figure 22 and the flat overall spectrum above 10 MeV in Figure 23 are suggestive of radiation from pion decay. The open symbols in Figures 22 and 23 are the 4.1–6.4 MeV fluences above the continuum (Chupp *et al.* 1983; Prince *et al.* 1983). The complete time profile of the 4.1–6.4 MeV flux from this flare (Chupp *et al.* 1983) is shown by the dashed curve in Figure 24. The corresponding time-integrated 4.1–6.4 MeV fluence is 305 photons cm^{-2} (Prince *et al.* 1983). The (42:44–43:49) period of Figure 22 coincides with the first large peak of the 4.1–6.4 MeV flux (14–78 s in Fig. 24). We identify this impulsive phase with the first phase of particle acceleration. The >10 MeV spectrum of the 1980 June 21 flare was observed only during the impulsive phase of the flare (see Forrest 1983 and Forrest *et al.* 1985). This spectrum is similar to that seen from the June 3 flare during the (42:44–43:49) period, except that it does not show the flattening above ~ 70 MeV. The time-integrated 4.1–6.4 MeV fluence for the June 21 flare is 76 photons cm^{-2} (Rieger *et al.* 1983).

The observed (Share *et al.* 1983) time profile of the 0.511 MeV line flux for the June 3 flare is shown in Figure 24. As can be seen, the peak of this flux occurs at about the same time (~ 150 s) as the second small peak of the 4.1–6.4 MeV flux, but there are no published 0.511 MeV data during the first large peak. The 0.511 MeV line data from the June 21 flare were given by Share *et al.* (1983). The 2.223 MeV line time profile and its total fluence, ~ 314 photons cm^{-2}, were given for the June 3 flare by Prince *et al.* (1983). The 2.223 MeV line fluence from the June 21 flare was ~ 3.1 photons cm^{-2} (Chupp 1982). This fluence is very small because in this limb flare the 2.223 MeV photons were strongly attenuated by Compton scattering in the photosphere.

The neutron observations were mentioned in § I. The yield function of the Jungfraujoch neutron monitor is shown in Figure 25 (Debrunner *et al.* 1983; E. Fluckiger 1986, private communication). The time-dependent count rates of this neu-

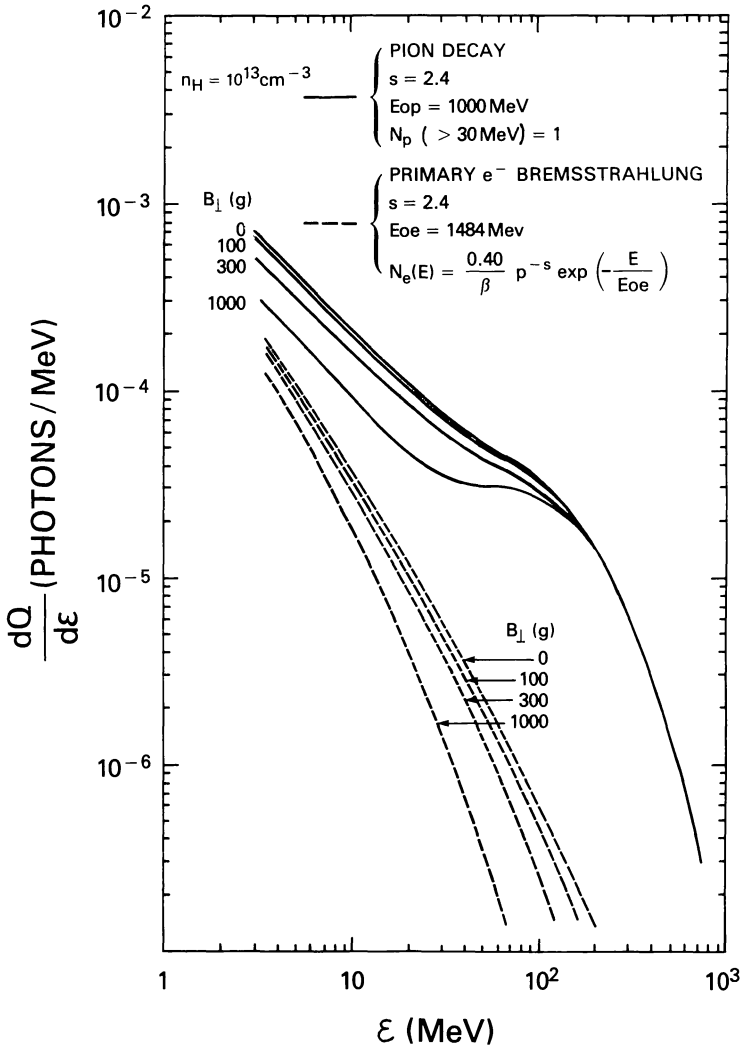

FIG. 20.—Effects of synchrotron losses on gamma-ray spectra from pion decay and primary electron bremsstrahlung for a variety of magnetic field strengths. The normalization of the primary electrons relative to the protons is such that at 3 MeV the fluxes of these two components are equal. This is consistent with the interplanetary observations of the June 3 flare (Fig. 2).

tron monitor are shown in Figure 26 (the same data are repeated in Figs. 27 and 29), and the neutron spectra inferred from the *SMM*/GRS observations and the interplanetary neutron-decay proton data are shown in Figure 28. The interplanetary charged particle observations were discussed in § II.

b) Implications of the 1980 June 21 Observations

The June 21 flare was analyzed previously (Murphy and Ramaty 1985). It was shown that a single energetic particle population having a stochastic-acceleration spectrum with $\alpha T = 0.025$ and $N_p(>30\ \text{MeV}) = 7.2\times10^{32}$ could simultaneously account for the neutron, the 4.1–6.4 MeV, and the 0.511 MeV line observations. Using this value of αT and the results of Figure 19, we find that the observed 4.1–6.4 MeV fluence of 76 photons cm^{-2} implies a differential fluence at 100 MeV from pion decay of 1.4×10^{-3} photons cm^{-2} MeV^{-1}. This is a factor of 6 lower than the observed flux at this energy, consistent with the unbroken power-law spectrum observed (Forrest *et al.* 1985) from the June 21 flare up to energies $\gtrsim$100 MeV. It was shown previously (Ramaty *et al.* 1983*b*) that the bulk of the gamma-ray emission above 10 MeV from this flare is due to primary electron bremsstrahlung. As can be seen from Figure 1, the observed interplanetary proton spectrum from this flare is consistent with the spectrum of protons that remain trapped at the Sun to produce the observed gamma rays and neutrons. Because the number of escaping particles, $N_{p,\text{esc}}(>30\ \text{MeV}) \approx 1.5\times10^{31}$ (§ II), is only $\sim 2\%$ of $N_p(>30\ \text{MeV})$, particle acceleration in this flare should take place in closed magnetic structures with little escape to interplanetary space. These structures are

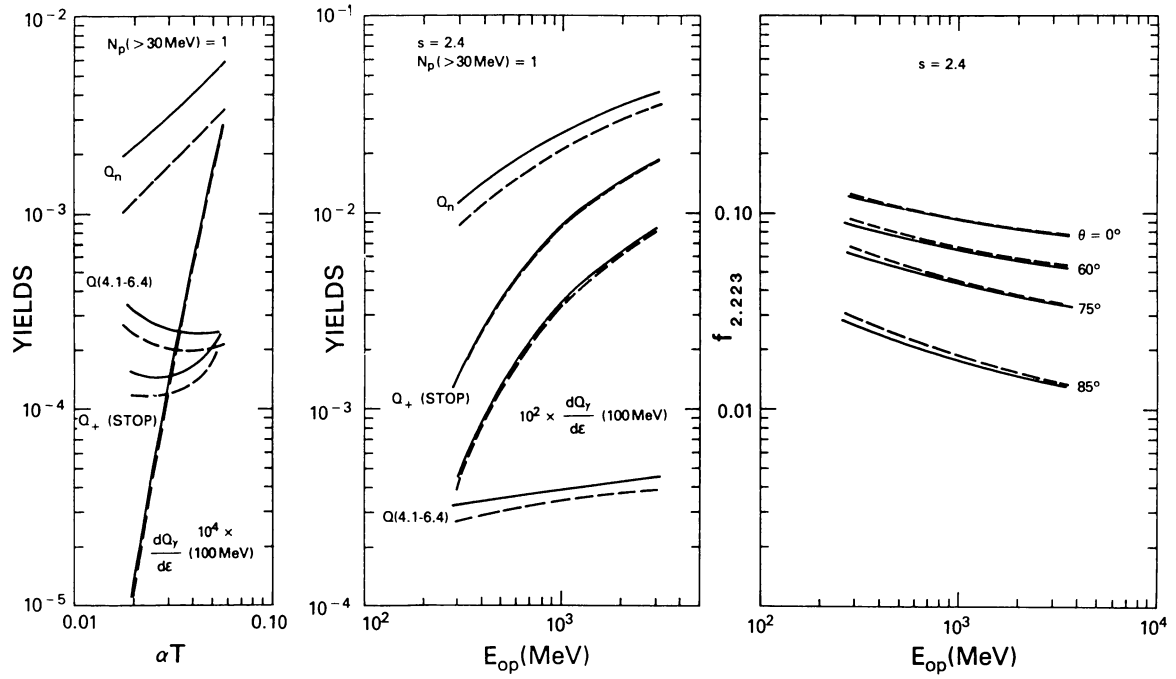

FIG. 21.—Total neutron, 4.1–6.4 MeV nuclear gamma-ray, and surviving (to produce a narrow 0.511 MeV line) positron yields, and the differential pion radiation yield at 100 MeV for stochastic- and shock-acceleration spectra. Also shown are the neutron–to–2.223 MeV photon conversion factors $f_{2.223}$ for shock-acceleration spectra, a variety of observation angles θ with respect to the normal to the photosphere, and isotropic neutron release above the photosphere (Wang 1975). Solid and dashed curves correspond to ambient and June 3 abundances for the accelerated particles.

probably loops. We identify this acceleration with first-phase acceleration.

c) *Implications of the 1982 June 3 Gamma-Ray Observations*

Particle acceleration in the June 3 flare, however, is more complex. For the period (42:44–43:49) the curve and histogram in Figure 22, representing photon spectra from pion decay and nuclear de-excitation, respectively, provide a good fit to the data. (The observations between ~10 and 70 MeV are probably due to bremsstrahlung of primary electrons.) These photon spectra are calculated (see § V) for a stochastic-acceleration particle spectrum with ambient medium abundance and $\alpha T = 0.04$. While the abundances have little effect on the ratio of the 4.1–6.4 MeV fluence to the differential fluence at 100 MeV, this ratio is strongly dependent on the shape of the spectrum. From Figure 19 we see that $\alpha T = 0.04$ gives the correct ratio. But this particle spectrum does not provide a good fit to the observed June 3 interplanetary proton spectrum (see Fig. 2). Conversely, the shock-acceleration spectrum which fits the interplanetary observations ($s = 2.4$, $E_{0p} > 300$ MeV) cannot account for the gamma-ray data in Figure 22. This can be seen from Figure 19, where values of $E_{0p} > 300$ MeV imply a ratio of $dQ/d\varepsilon$(100 MeV) to Q(4.1–6.4 MeV) larger than that observed by at least a factor of 25. Thus, the particles interacting at the Sun to produce the gamma rays during the (42:44–43:49) period and the particles seen in interplanetary space probably have different origins. The normalization of the calculated spectra in Figure 22 yields $N_p(>30\text{ MeV}) \approx 2.5\times10^{33}$. If the density of the ambient medium exceeds $\sim 10^{13}$ cm^{-3}, the pion-decay radiation is produced on a time scale shorter than the observation period (see § V). Then the value of N_p is essentially the number of protons interacting during this period.

For the (46:00–47:06) period, the observed photon spectrum (Fig. 23) is much harder than for the earlier (42:44–43:49) period. A stochastic-acceleration spectrum with $\alpha T = 0.04$, therefore, can no longer account for the observations. This is seen in Figure 23, where the solid curve falls below the observations at 100 MeV by a factor of ~30. On the other hand, the shock-acceleration spectrum which fits the interplanetary observations does provide a good fit to the data. The dashed curve in Figure 23 is radiation from pion decay produced by energetic particles with $s = 2.4$, $E_{0p} = 1000$ MeV, and the observed June 3 composition (Table 1). This value of E_{0p} is larger than the minimum value of 300 MeV (see § II) and close to the maximum value determined (see below) from observations (Debrunner *et al.* 1983; E. Fluckiger 1986, private communication) with the Jungfraujoch neutron monitor, which is very sensitive to high-energy neutrons. The normalization of the dashed curve to the data yields $N_p(>30\text{ MeV}) \approx 4.2\times10^{30}$ for this period. Comparison with Figure 20 indicates that for $n_H > 10^{13}$ cm^{-3}, $B_\perp$ should be less than ~300 G; otherwise the gamma rays would be excessively suppressed by synchrotron losses of the positrons and electrons. Based on the primary electron-to-proton ratio derived

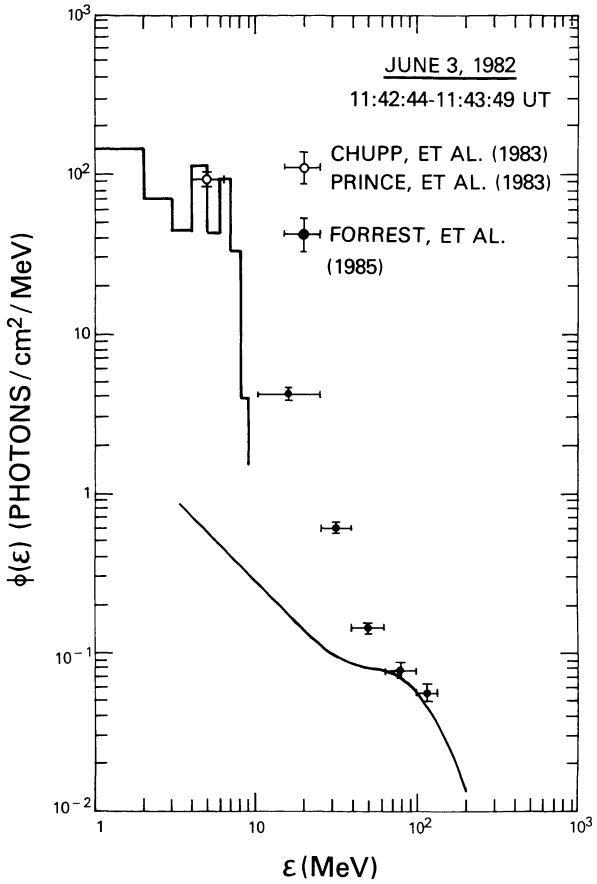

FIG. 22.—Gamma radiation from the 1982 June 3 flare during the time interval 11:42:44–11:43:49 UT. *Solid curve*: pion-decay gamma radiation expected from a stochastic-acceleration spectrum with ambient composition, $\alpha T = 0.04$ and $N_p(>30\ \text{MeV}) = 2.5\times10^{33}$; *histogram*: associated gamma-ray line radiation assuming 1 MeV detector resolution. Sources of the data are indicated and discussed in the text.

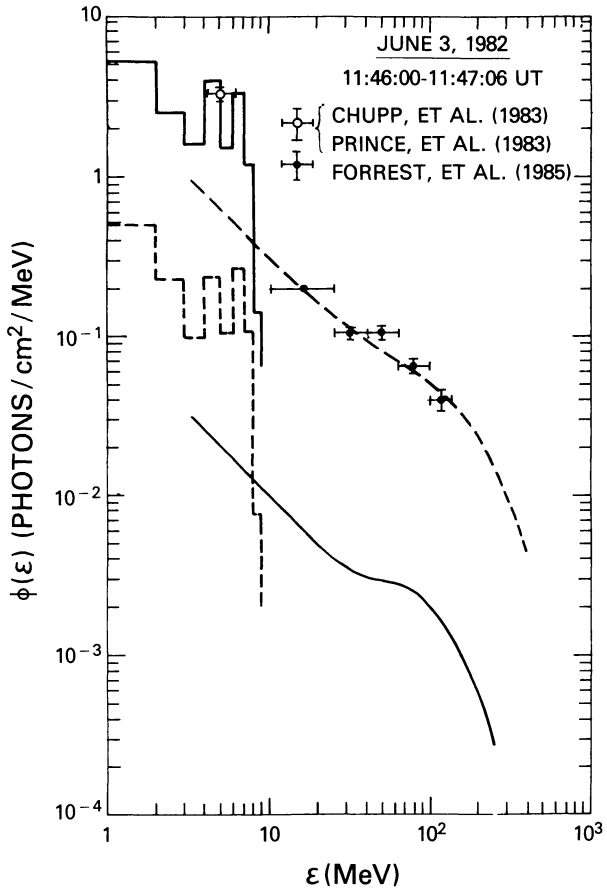

FIG. 23.—Same as Fig. 22, but for observations in the time interval 11:46:00–11:47:06 UT. Solid curve and histogram refer to a stochastic-acceleration spectrum with ambient composition, $\alpha T = 0.04$, and $N_p(>30\ \text{MeV}) = 8.8\times10^{31}$. Dashed curve and histogram refer to a shock-acceleration spectrum with June 3 composition, $s = 2.4$, $E_{0p} = 1000$ MeV, and $N_p(>30\ \text{MeV}) = 4.2\times10^{30}$.

from the interplanetary observations, the contribution of primary electron bremsstrahlung to the data shown in Figure 23 is much smaller than that of the pion-decay radiation (see Fig. 20).

The dashed histogram in Figure 23 is the nuclear gamma-ray emission produced by the shock-acceleration spectrum with the same parameters. As can be seen, this emission is insufficient to account for the observed 4.1–6.4 MeV fluence. Even if the value of E_{0p} were equal to the lower limit set by the interplanetary observations (300 MeV), we see from Figure 19 that these particles could only produce about half of the 4.1–6.4 MeV fluence observed during the (46:00–47:06) period. Thus, while the >10 MeV data in Figure 23 cannot be produced by the stochastic-acceleration spectrum with $\alpha T = 0.04$, the nuclear line emission could be a combination of contributions from this spectrum and the shock-acceleration spectrum.

Having attributed the production of the 4.1–6.4 MeV fluence in the (42:44–43:49) period to the stochastic-acceleration spectrum, we assume for simplicity that all of the observed 4.1–6.4 MeV fluence is produced by such particles, even though at later times, as we have just seen, the shock-acceleration spectrum could make an important contribution. This, however, does not introduce too much uncertainty into the calculations, since the 4.1–6.4 MeV fluence observed in the (42:44–43:49) period amounts to ~ 70% of the total. We then obtain $N_p(>30\ \text{MeV}) \approx 3.5\times10^{33}$, where this is the total number of protons in the stochastic-acceleration component interacting at the Sun. We associate these protons with acceleration in the first phase. While stochastic acceleration is consistent with the data, we point out that other mechanisms, including shock acceleration with an E_{0p} value less than the lower limit set by the interplanetary observations, could also account for the observations.

The solid curve 2 in Figure 24 is the time profile of the 0.511 MeV line produced by this first-phase stochastic-acceleration spectrum with $\alpha T = 0.04$, $N_p(>30\ \text{MeV}) = 3.5\times10^{33}$, and time dependence as given by the dashed curve in the figure. The time profile of curve 2 is determined mainly by delayed positron production from radioactive beta emitters and is quite insensitive to the detailed time dependence of the stochastic-acceleration component. Curve 3 in Figure 24, the difference between curve 1 (a smooth fit through the data) and curve 2, should represent the contribution of the shock-accel-

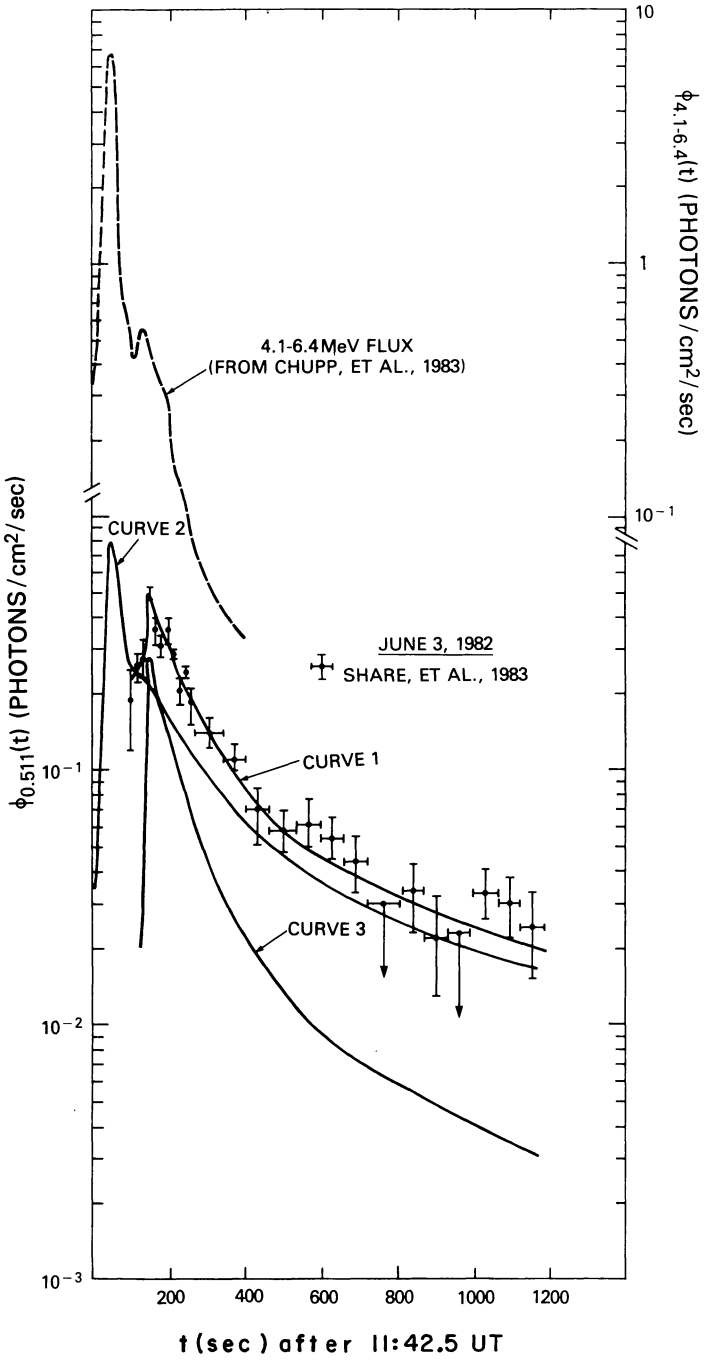

FIG. 24.—Time dependences for the 1982 June 3 flare. *Dashed curve*: observed time dependence of the 4.1–6.4 MeV excess. *Curve 1*: fit to the observed 0.511 MeV flux. *Curve 2*: calculated 0.511 MeV flux for a stochastic-acceleration spectrum with $\alpha T = 0.04$, $N_p(>30\ \text{MeV}) = 3.5\times10^{33}$, time dependence as given by the dashed curve, and ambient composition. *Curve 3*: difference between curve 1 and curve 2, representing the contribution of the shock-acceleration component.

eration spectrum to the total 0.511 MeV line emission. As a check on this hypothesis, we calculate the 0.511 MeV line emission produced by the shock-acceleration spectrum during the (46:00–47:06) period using the parameters derived by fitting the >10 MeV emission in Figure 23. We find $\phi_{0.511}(210\text{–}276\ \text{s}) \approx 0.13$ photons cm^{-2} s^{-1}, in good agreement with the flux given by curve 3. During the (42:44–43:49) period, the positron emitters are produced only by the stochastic-acceleration spectrum (curve 2). This implies that the shock-acceleration spectrum produces significant nuclear reactions only after this period, suggesting that shock acceleration begins after the maximum of the 4.1–6.4 MeV emission. We associate curve 3 with the time profile of interactions produced by particles accelerated in the second phase. Using

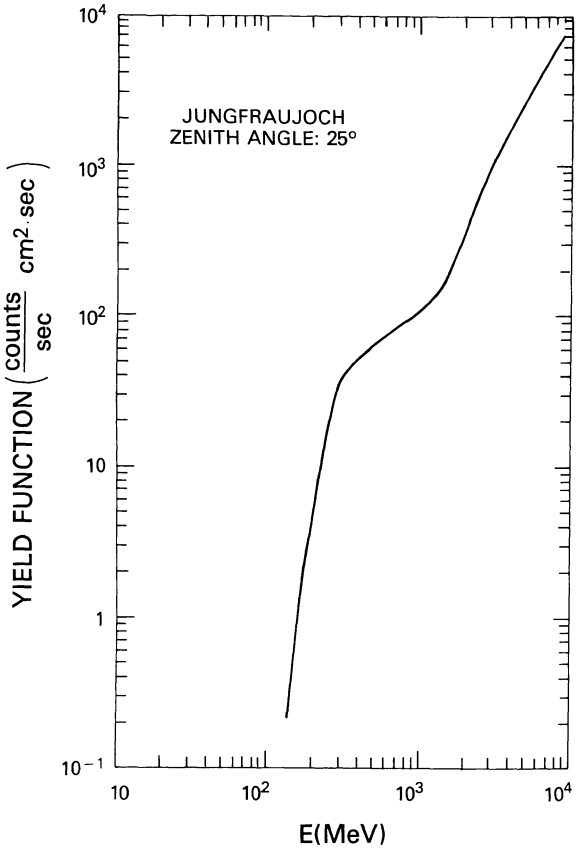

FIG. 25.—Yield function of the Jungfraujoch neutron monitor (Debrunner *et al.* 1983; E. Fluckiger 1986, private communication).

this time profile, we obtain the total numbers of protons accelerated in this phase, $N_p(>30\ \mathrm{MeV}) \approx 2.0\times10^{31}$.

The parameters of the particle populations resulting from the two phases can now be compared with each other and with the parameters of the particles observed in interplanetary space. From the gamma rays we have $N_p(>30\ \mathrm{MeV}) \approx 3.5\times10^{33}$ and $\alpha T \approx 0.04$ for the first phase, and $N_p(>30\ \mathrm{MeV}) \approx 2.0\times10^{31}$, $s \approx 2.4$, and $E_{0p} \approx 1000$ MeV for the second. From the interplanetary observations, $N_{p,\mathrm{esc}}(>30\ \mathrm{MeV}) \approx 3\times10^{32}$, $s \approx 2.4$ and $E_{0p} > 300$ MeV (§ II). Thus, first-phase acceleration produces a significantly steeper proton spectrum than does the second, and the interplanetary proton spectrum is consistent with that produced in the second phase and probably inconsistent with that resulting from the first. Furthermore, the number of interplanetary protons is smaller than the number of interacting protons resulting from the first phase, but considerably larger than the number of interacting protons resulting from the second. These results can be understood most easily if first-phase acceleration takes place in closed loops with little escape to interplanetary space, while second-phase acceleration occurs on open magnetic structures such that the bulk of the accelerated particles escape. Thus, the June 3 flare is similar to that of June 21, in that first-phase acceleration with little particle escape occurred in both flares. But it is different because of the additional second phase, which, by producing a very flat proton spectrum, had a distinctive pion signature.

d) *Applications to the 1982 June 3 Neutron Observations*

Using the parameters and time profiles of the two populations derived above, we have evaluated the time- and energy-dependent neutron flux at Earth. We first compare the results with the Jungfraujoch neutron monitor observations. Using the neutron monitor yield function shown in Figure 25, we compare in Figure 26 the expected and observed count rates, and we see that there is reasonable agreement. However, if we repeat the calculations with $E_{0p} = 3000$ MeV, we see in Figure 27 that the expected count rate is much larger than that observed and that the discrepancy is entirely due to the shock-acceleration spectrum. Thus E_{0p} should not exceed $\sim$1000 MeV. We note that the fit of the calculated curve in Figure 26 to the Jungfraujoch data at 11:53–11:55 UT is not very good. While we have not explored this possibility in detail, we estimate that because of the extreme sensitivity of the neutron monitor to high-energy neutrons, a sudden increase in E_{0p} just prior to this time interval could increase the count rate without significantly affecting the 0.511 MeV line flux.

We compare the calculations with the other neutron observations in Figure 28. Since the *SMM*/GRS detector does not measure neutron energy, this spectrum was obtained (Chupp *et al.* 1983) from the arrival time of the neutrons and the assumption that the neutrons were produced instantaneously at 11:43:26 UT (i.e., at the peak of the 4.1–6.4 MeV flux). The Evenson, Meyer, and Pyle (1983) spectrum follows directly from the observed spectrum of the neutron-decay protons in interplanetary space. Curve 1 is the total neutron spectrum obtained by combining the contributions of shock acceleration (shown by curve 3) and stochastic acceleration using the parameters given above. We see that at low energies the stochastic-acceleration component dominates, while at high energies the shock-acceleration component becomes important. We have also calculated the 2.223 MeV line fluence resulting from the total neutron spectrum using neutron–to–2.223 MeV photon conversion factors as discussed by Murphy and Ramaty (1985) and also given in Figure 21. We obtain $\phi_{2.223} \approx 412$ photons cm^{-2}. The fact that for the isotropic proton distributions used throughout the paper this value is somewhat larger than the observed fluence ($\sim$314 photons cm^{-2}) rules out a strongly downward-peaked proton distribution (see § II).

Neutron production can be lowered relative to the various gamma-ray channels by lowering the relative abundance of the alpha particles (see Fig. 21). To investigate the effects of such a variation, we have modified the composition of the stochastic-acceleration component from the ambient medium composition to the June 3 composition (Table 1). Keeping the spectral parameters constant and adjusting the values of N_p so that the pion-decay emission, the nuclear gamma rays, and the 0.511 MeV line flux remain unchanged, we obtain $\phi_{2.223} \approx$ 326 photons cm^{-2}, curve 2 in Figure 28, and the neutron monitor count rate shown in Figure 29. The value of $N_p(>30$

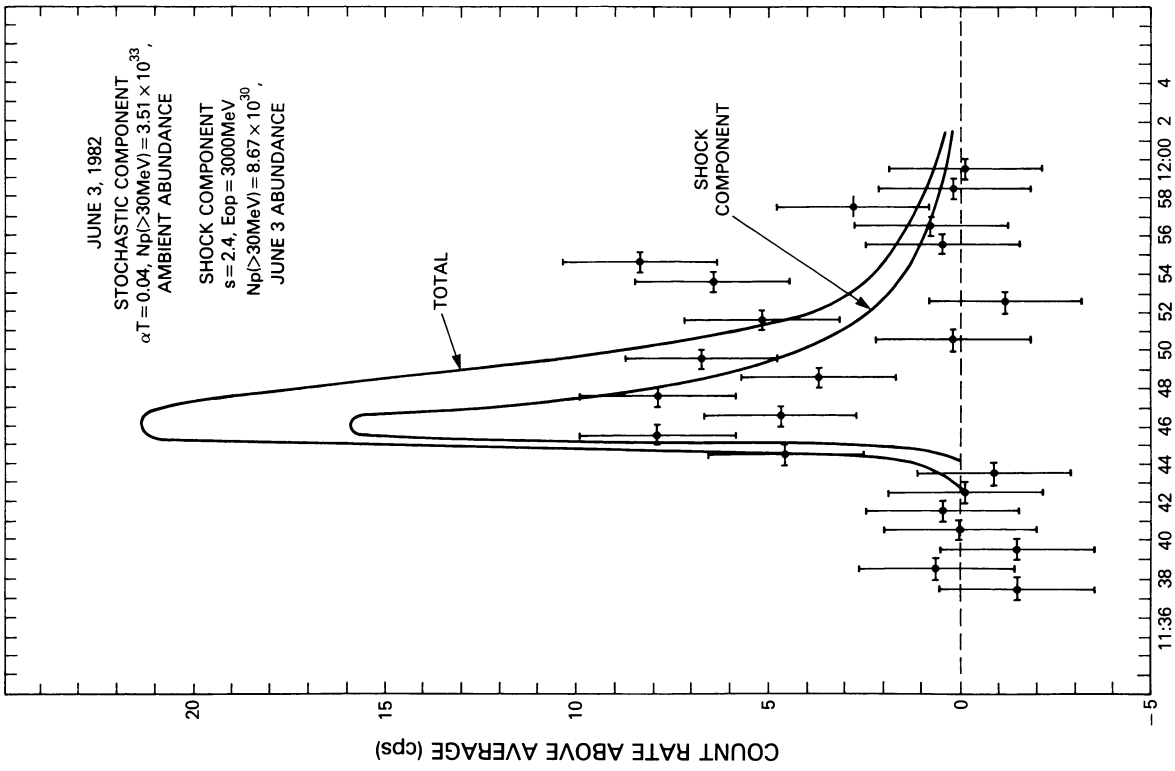

FIG. 27

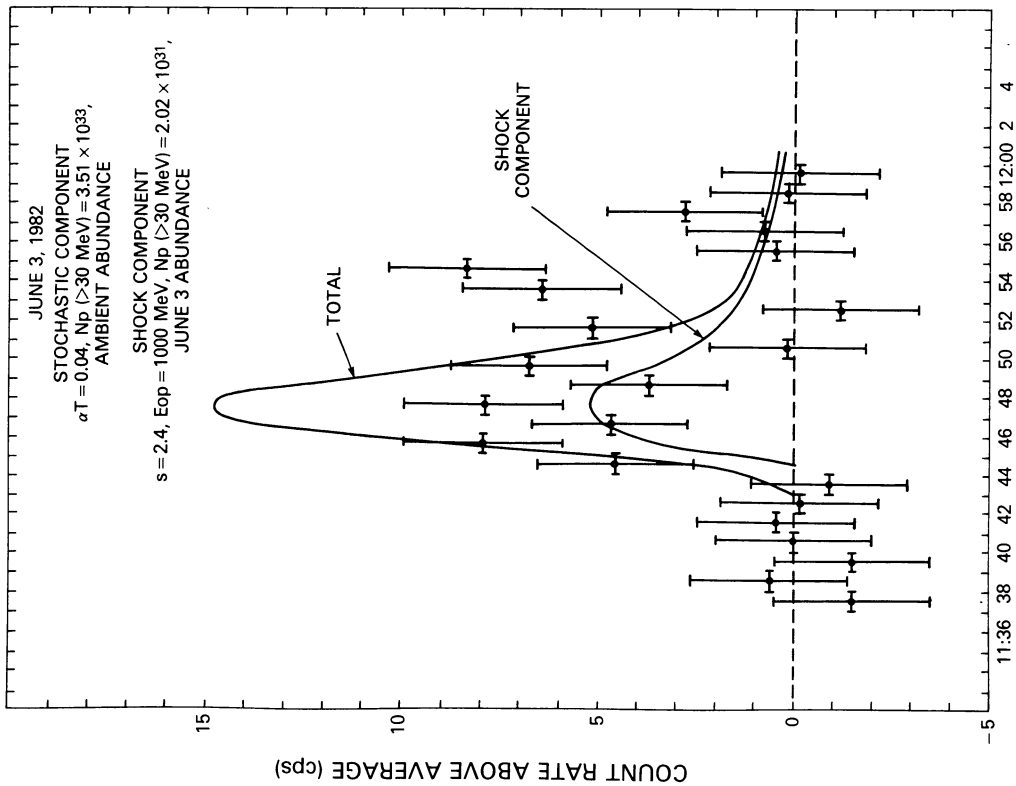

FIG. 26

FIG. 26.—Observed and calculated neutron monitor count rates. Data from H. Debrunner (1986, private communication).

FIG. 27.—Observed and calculated neutron monitor count rates. Origin of data as in Fig. 26.

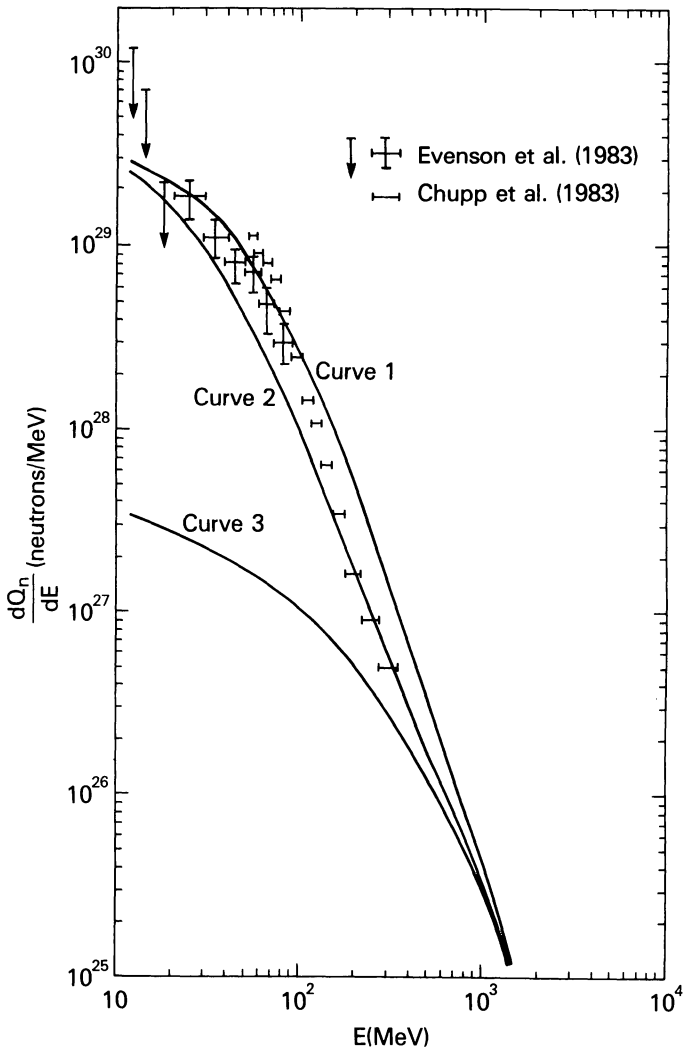

FIG. 28

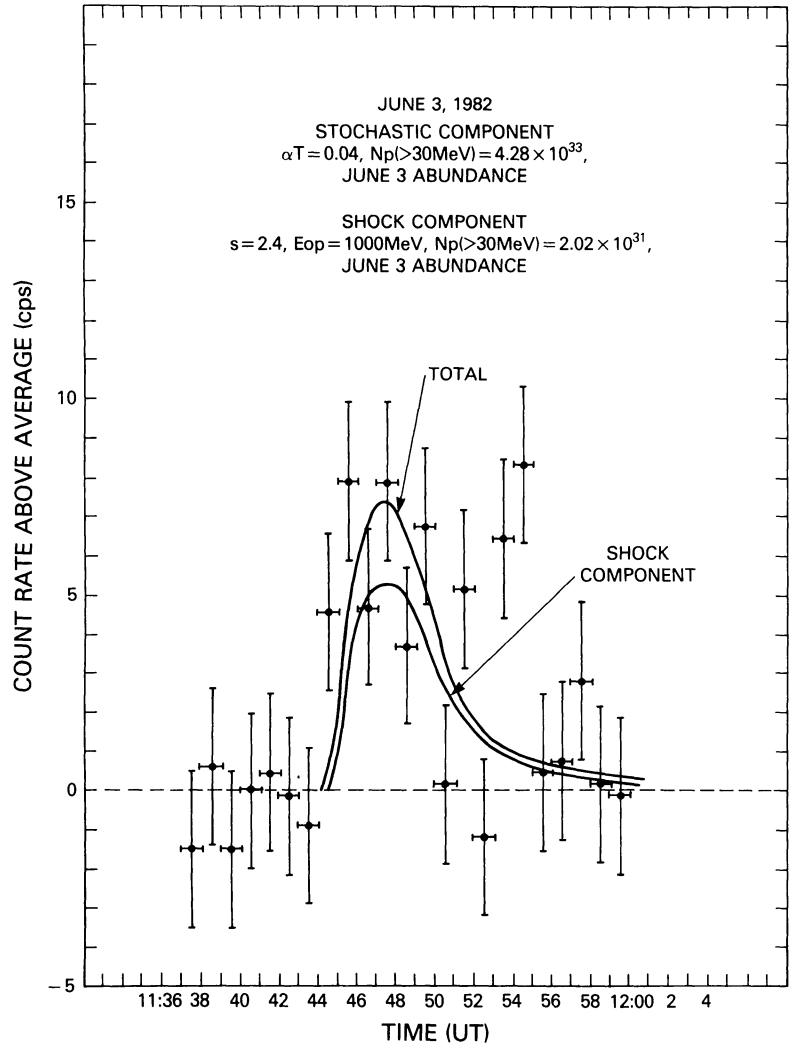

FIG. 29

FIG. 28.—Observed and calculated neutron energy spectra for the 1982 June 3 flare. Curves 1 and 2 were calculated for the parameters given in Figs. 26 and 29, respectively. Curve 3 is the contribution of the shock-acceleration component with parameters as given in either Fig. 26 or Fig. 29.

FIG. 29.—Observed and calculated neutron monitor count rates. Origin of data as in Fig. 26.

MeV) is now 4.3×10^{33} for the stochastic-acceleration spectrum and unchanged (2.0×10^{31}) for the shock-acceleration spectrum. We see that variations in the composition do have a strong effect on the neutron yields, with the extreme cases bracketing the observations.

Returning to the results of Figure 26, we see that the second-phase shock component makes an important contribution which is very sensitive to E_{0p}, as can be seen from a comparison of Figures 26 and 27. We note that the neutron monitor data can be reliably analyzed only if the energies of the neutrons impinging on the atmosphere of the Earth are known, since the neutron monitor does not measure the neutron energy, but its yield is very sensitive to this energy. It has been the approach of the present study to constrain the particle energy spectra by using the gamma-ray observations and to confront the resultant neutron spectra with the observations.

VII. SUMMARY

Our principal results are as follows:

1. There is good evidence for radiation from pion decay in the 1982 June 3 flare. Early in the life history of the flare, when bremsstrahlung from primary electrons is still very important, this radiation manifests itself as a spectral flattening at energies above ~ 70 MeV. We have shown that later in the flare, the pion-decay radiation dominates the primary electron bremsstrahlung at all energies above 10 MeV. This result is based on a detailed calculation of the radiation expected from neutral and charged pion decay and on the primary electron bremsstrahlung inferred from the electron-to-proton ratio observed in interplanetary particles.

2. The comparison of the pion-decay radiation with the radiation from nuclear de-excitation rules out gamma-ray production in the 1982 June 3 flare by a single particle population whose energy spectrum is time-independent. The ratio of the fluxes of these two radiations is strongly dependent on the proton energy spectrum because the nuclear lines are produced predominantly by lower energy protons (10–100 MeV), while the pions result from protons above at least several hundred MeV. We find that early in the flare, when the nuclear line-to-pion ratio is high, the proton spectrum is too steep to be consistent with the very hard interplanetary proton spectrum observed from the June 3 flare. Later in the flare, however, the spectrum of the protons interacting at the Sun is much flatter and consistent with the interplanetary observations. While the interplanetary observations require that the high-energy turnover, E_{0p}, exceeds ~ 300 MeV, the Jungfraujoch neutron monitor data imply that $E_{0p} \lesssim 1000$ MeV.

3. On the basis of these results, we suggest that two distinct particle populations were accelerated in the June 3 flare. We identify the first population with acceleration in a first phase whose definition was given originally by Wild, Smerd, and Weiss (1963) and further elaborated on the basis of the *SMM*/GRS observations. These observations demonstrated that proton acceleration is a common characteristic of the first phase. We relate the second population to the second phase of Wild, Smerd, and Weiss, in which acceleration is probably due to shocks in the corona.

4. In the June 3 flare, the first-phase protons produce the bulk of the observed 4.1–6.4 MeV and 2.223 MeV fluences. On the other hand, more pion-decay radiation results from protons accelerated in the second phase. Second-phase protons also make an important contribution to the highest energy neutron flux at Earth observed with ground-based neutron monitors. The 0.511 MeV line flux consists of approximately equal contributions from the two phases, with radioactive beta emitters being the dominant positron source in the first phase and positive pion decay in the second.

5. In the 1980 June 21 flare the observed gamma rays and neutrons were produced in only a single phase. This flare exhibited the strong 4.1–6.4 MeV emission expected from the first phase and had delayed 0.511 MeV line emission resulting from radioactive beta emitters produced along with the 4.1–6.4 MeV emission, but did not produce observable radiation from pion decay.

6. Regarding the relationship between the interacting protons at the Sun and the protons observed in interplanetary space, our conclusions are consistent with the results of Cane, McGuire, and von Rosenvinge (1986) and Bai (1986), namely, that the bulk of the first-phase gamma-ray–producing protons remain trapped at the Sun and the majority of the second-phase protons escape. While the first-phase component is seen from essentially all gamma-ray flares, the second-phase gamma-ray signature has so far been observed only from the 1982 June 3 flare.

We wish to thank H. Debrunner and E. Fluckiger for providing us the Jungfraujoch neutron monitor data, and B. Kozlovsky for assistance in assembling and analyzing the neutron production cross sections. R. J. M. acknowledges financial support from NASA/GSFC grant 5-1268.

REFERENCES

Badhwar, G. D., Stephens, S. A., and Golden, R. L. 1977, *Phys. Rev. D*, **15**, 820.
Bai, T. 1986, *Ap. J.*, **308**, 912.
Barkas, W. H., and Berger, M. J. 1964, *Tables of Energy Losses and Ranges of Heavy Charged Particles*, NASA SP-3013.
Berger, M. J., and Seltzer, S. M. 1964, *Tables of Energy Losses and Ranges of Electrons and Positrons*, NASA SP-3012.
Brown, B. L., Leventhal, M., Mills, A. P., Jr., and Gidley, D. W. 1984, *Phys. Rev. Letters*, **53**, 2347.
Bugg, D. V., *et al.* 1964, *Phys. Rev.*, **133**, B1017.
Bugg, D. V., Salter, D. C., Stafford, G. H., George, R. F., Riley, K. F., and Tapper, R. J. 1966, *Phys. Rev.*, **123**, 980.
Cameron, A. G. 1982, in *Essays in Nuclear Astrophysics*, ed. C. Barnes, D. D. Clayton, and D. N. Schramm (Cambridge: Cambridge University Press), p. 23.
Cane, H. V., McGuire, R. E., and von Rosenvinge, T. T. 1986, *Ap. J.*, **301**, 448.
Cavallo, G., and Gould, R. J. 1971, *Nuovo Cimento*, **2B**, 77.
Chupp, E. L. 1982, in *Gamma-Ray Transients and Related Astrophysical Phenomena*, ed. R. E. Lingenfelter, H. S. Hudson, and D. M. Worrall (New York: AIP), p. 363.
_____. 1984, *Ann. Rev. Astr. Ap.*, **22**, 359.
Chupp, E. L., Forrest, D. J., Kanbach, G., Share, G. H., Debrunner, H., and Fluckiger, E. 1983, *Proc. 18th Internat. Cosmic Ray Conf.* (Bangalore), **10**, 334.
Chupp, E. L., *et al.* 1982, *Ap. J.* (*Letters*), **273**, L95.
Cochran, D. R. F., *et al.* 1972, *Phys. Rev. D*, **6**, 3085.
Crannell, C. J., Crannell, H., and Ramaty, R. 1979, *Ap. J.*, **229**, 762.
Crawford, J. F., *et al.* 1980, *Phys. Rev. C*, **22**, 1184.

Debrunner, H., Fluckiger, E., Chupp, E. L., and Forrest, D. J. 1983, *Proc. 18th Internat. Cosmic Ray Conf.* (Bangalore), **4**, 75.
Dermer, C. D. 1986*a*, *Ap. J.*, **307**, 47.
_____. 1986*b*, *Astr. Ap.*, **157**, 223.
Dermer, C. D., and Ramaty, R. 1986, *Ap. J.*, **301**, 962.
Efimov, Yu. E., and Kocharov, G. E. 1985, *Proc. 19th Internat. Cosmic Ray Conf.* (La Jolla), **4**, 154.
Efimov, Yu. E., Kocharov, G. E., and Kudela, K. 1983, *Proc. 18th Internat. Cosmic Ray Conf.* (Bangalore), **10**, 276.
Ellison, D. C., and Ramaty, R. 1985, *Ap. J.*, **298**, 400.
Evenson, P., Meyer, P., and Pyle, K. R. 1983, *Ap. J.*, **274**, 875.
Forman, M. A., Ramaty, R., and Zweibel, E. G. 1986, in *The Physics of the Sun*, Vol. **2**, ed. P. A. Sturrock, T. E. Holzer, D. Mihalas, and R. K. Ulrich (Dordrecht: Reidel), p. 249.
Forrest, D. J. 1983, in *Positron and Electron Pairs in Astrophysics*, ed. M. L. Burns, A. K. Harding, and R. Ramaty (New York: AIP), p. 3.
Forrest, D. J. *et al.* 1981, *Proc. 17th Internat. Cosmic Ray Conf.* (Paris), **10**, 5.
Forrest, D. J., Vestrand, W. T., Chupp, E. L., Rieger, E., Cooper, J., and Share, G. 1985, *Proc. 19th Internat. Cosmic Ray Conf.* (La Jolla), **4**, 146.
Ginzburg, V. L., and Syrovatskii, S. I. 1964, *The Origin of Cosmic Rays* (New York: Macmillan).
Glagola, B. G., Viola, V. E., Breuer, H., Chant, N. S., Nadasen, A., Roos, P. G., Austin, S. M., and Mathews, G. J. 1982, *Phys. Rev. C*, **25**, 34.
Handler, R. 1965, *Phys. Rev. B*, **138**, 1230.
Heitler, W. 1957, *The Quantum Theory of Radiation* (London: Oxford University Press).
Hua, X.-M., and Lingenfelter, R. E. 1987, *Ap. J.*, submitted.
Iucci, N., Parisi, M., Signorini, C., Storini, M., and Villoresi, G. 1984, *Nuovo Cimento*, **7C**, 732.
Kocharov, G. E. 1983, *Bull. Acad. Sci. USSR, Phys. Ser.*, **47**, 44.
Kozodaev, M. S., Kulyukin, M. M., Sulyaev, R. M., Filipov, A. I., and Shcherbakov, Yu. A. 1960, *Soviet Phys.—JETP*, **38**, 511.
Lebedev, A. M., Slavatinskii, S. A., and Tolkachev, B. V. 1963, *Soviet Phys.—JETP*, **19**, 1452.
Lindenbaum, S. J., and Sternheimer, R. M. 1957, *Phys. Rev.*, **105**, 1874.
Lingenfelter, R. E., Flamm, E. J., Canfield, E. H., and Kellman, S. 1965, *J. Geophys. Res.*, **70**, 4077, 4087.
Lock, W., and Measday, D. F. 1970, *Intermediate Energy Nuclear Physics* (London: Methuen).
McDonald, F. B., and Van Hollebeke, M. A. I. 1985, *Ap. J.* (*Letters*), **290**, L67.
McGuire, R. E., von Rosenvinge, T. T., and McDonald, F. B. 1986, *Ap. J.*, **301**, 938.
Meyer, J. P. 1972, *Astr. Ap. Suppl.*, **7**, 417.
Murphy, R. J. 1985, Ph.D. thesis, University of Maryland.
Murphy, R. J., Forrest, D. J., Ramaty, R., and Kozlovsky, B. 1985*b*, *Proc. 19th Internat. Cosmic Ray Conf.* (La Jolla), **4**, 253.
Murphy, R. J., and Ramaty, R. 1985, *Advances in Space Research* (COSPAR), Vol. **4**, No. 7, p. 127.
Murphy, R. J., Ramaty, R., Forrest, D. J., and Kozlovsky, B. 1985*a*, *Proc. 19th Internat. Cosmic Ray Conf.* (La Jolla), **4**, 249.
Orth, C. D., and Buffington, A. 1976, *Ap. J.*, **206**, 312.
Paic, G., Antolkovic, B., Djaloeis, A., Bojowald, J., and Mayer-Boricke, C. 1981, *Phys. Rev. C*, **24**, 841.
Particle Data Group. 1984, *Rev. Mod. Phys.*, **56**, S70.
Perl, M. L. 1974, *High Energy Hadron Physics* (New York: Wiley), p. 169.
Petrosian, V. 1985, *Ap. J.*, **299**, 987.
Prince, T. A., Forrest, D. J., Chupp, E. L., Kanbach, G., and Share, G. H. 1983, *Proc. 18th Internat. Cosmic Ray Conf.* (Bangalore), **4**, 79.
Prokoshkin, Iu. D., and Tiapkin, A. A. 1958, *Soviet Phys.—JETP*, **5**, 618.
Ramaty, R. 1979, in *Particle Acceleration Mechanisms in Astrophysics*, ed. J. Arons, C. Max, and C. McKee (New York: AIP), p. 135.
_____. 1986, in *The Physics of the Sun*, Vol. 2, ed. P. A. Sturrock, T. E. Holzer, D. Mihalas, and R. K. Ulrich (Dordrecht: Reidel), p. 291.
Ramaty, R., Kozlovsky, B., and Lingenfelter, R. E. 1975, *Space Sci. Rev.*, **18**, 341.
_____. 1979, *Ap. J. Suppl.*, **40**, 487.
Ramaty, R., and Lingenfelter, R. E. 1969, *Ap. J.*, **155**, 587.
Ramaty, R., Murphy, R. J., Kozlovsky, B., and Lingenfelter, R. E. 1983*a*, *Solar Phys.*, **86**, 395.
_____. 1983*b*, *Ap. J.* (*Letters*), **273**, 141.
Riddiford, L., and Williams, A. W. 1960, *Proc. Roy. Soc. London*, *A*, **257**, 316.
Rieger, E., Reppin, C., Kanbach, G., Forrest, D. J., Chupp, E. L., and Share, G. H. 1983, *Proc. 18th Internat. Cosmic Ray Conf.* (Bangalore), **10**, 338.
Share, G. H., Chupp, E. L., Forrest, D. J., and Rieger, E. 1983, in *Positron and Electron Pairs in Astrophysics*, ed. M. L. Burns, A. K. Harding, and R. Ramaty (New York: AIP), p. 15.
Stecker, F. W. 1970, *Ap. Space Sci.*, **6**, 377.
Stephens, S. A., and Badhwar, G. D. 1981, *Ap. Space Sci.*, **76**, 213.
Tan, L. C., and Ng, L. K. 1982, *Phys. Rev. D*, **26**, 1179.
_____. 1983, *J. Phys. G*, **9**, 1289.
Tannenwald, P. O. 1953, *Phys. Rev.*, **89**, 508.
Van Hollebeke, M. A. I., McDonald, F. B., and Trainor, J. H. 1985, *Proc. 19th Internat. Cosmic Ray Conf.* (La Jolla), **4**, 209.
Vlahos, L., *et al.* 1986, in *Energetic Phenomena on the Sun*, ed. M. R. Kundu and B. Woodgate (NASA Conf. Rept.), in press.
Wang, H. T. 1975, Ph.D. thesis, University of Maryland.
Wang, H. T., and Ramaty, R. 1974, *Solar Phys.*, **36**, 129.
Wild, J. P., Smerd, S. F., and Weiss, A. A. 1963, *Ann. Rev. Astr. Ap.*, **1**, 291.

CHARLES D. DERMER: Lawrence Livermore National Laboratory, P.O. Box 808, L-421, Livermore, CA 99550

RONALD J. MURPHY: Code 4154, Naval Research Laboratory, Washington, DC 20375

REUVEN RAMATY: Code 665, NASA/Goddard Space Flight Center, Greenbelt, MD 20771